An Investigation into the Development of a Miniature Piezoelectric Pump

Lei Meng

Thesis submitted in full fulfillment of the degree of Master of Engineering

Auckland University of Technology

Auckland

New Zealand

Primary supervisor Prof. Ahmed Al-Jumaily

Second supervisor Dr. Maximiano Ramos

To my dear parents,

DingYi Meng and GuiJu Gao

Acknowledgements

Firstly, I would like to express my sincere appreciation to my Primary supervisor Prof. Ahmed Al-Jumaily and Second supervisor Dr. Maximiano Ramos for their support and guidance this project. It's also generous and friendship, combined with unlimited patience has enabled me to finish this project.

Secondly, I would also like to say a "Thank you" to Brett Holden, Stephen Hartley, Ross Reichardt, Mark Masterton and Bradley Scott, technicians at Auckland University of Technology, for their helping me during the manufacturing phase of this project. And say a big "Thank you" to Prof. Olaf Diegel, who helped me greatly on the Solid-Work Software, without your professional skills I might haven't finished my prototype design so quickly.

Next I would like to thank my colleague Master students Lei Wang, Pablo Brizio and Mark Hildesly. Without your endless jokes, chats and friendship, my lab times won't be such a fun place to work in.

Finally, I would also like to thank my dear families, who are far away in distance but so close to my heart. And most importantly, I must thank my dear girlfriend Shwu Chyi Ng (Janice Ng), for her understanding, support and encouragement at distance.

Table of Contents

Table of Figures

Abstract

This thesis is aimed at improving the understanding and effectiveness in operating of the micropump in CPAP system. The principle objectives were to understand the air flow rate and air pressure of a micropump designs for the CPAP System.

The feasibility of developing a micropump using piezoelectric fans was investigated. Input frequencies and voltages were quantified for different chambers of micropump, discharge air flow rates and air pressure. The effect of these parameters on flow rate and air pressure was determined.

To test the effect of air flow and air pressure produced by the micropump, a mathematical model of piezoelectric fan is developed.

The experimental results with dynamic characteristics of air flow resulted in the following conclusions.

- The vibration frequency is influential in determining the attainable pressure compared to the vibration amplitude.
- The parallel configuration of two piezoelectric fans excited with the same phase yields more flow rate than excited with opposite phase. The parallel configuration yields more flow rate than series configuration, but the series configuration yields higher air pressure.
- The shapes of the flow channel, inlet and outlet have significant influence on the air flow rate and pressure.

Chapter 1 Introduction

1.1 Background

Obstructive Sleep Apnea Syndrome (OSAS) is a common disorder which affects a significant part of the population. OSAS is characterized by repetitive episodes of upper airway obstruction (apnoea) or narrowing (hypopnea) as show in Figure 1.1. For instance 4% of men and 2% of women in middle aged US population **[1]**, 4.1-7.5% of men and 2.1- 3.2% of woman in the same age-ranged Asian population **[2, 3]** and 7.5% in Indian men suffer OSAS**[4]**, affect over 35 million people in the world. New Zealand has a higher rate than many countries with about 6% of adults aged between 30 and 60 suffer from OSA and 80% of those are undiagnosed. This is more prevalent in the Maori and Pacific populations as most likely those are overweight, have high cholesterol, high blood pressure and some abnormality in the upper airway **[5]**. The consequences include respiratory disturbances from significant obstruction with or without reduced airflow (Hypopnoea and Snoring) to total absence of airflow (Apnea) **[6]**.

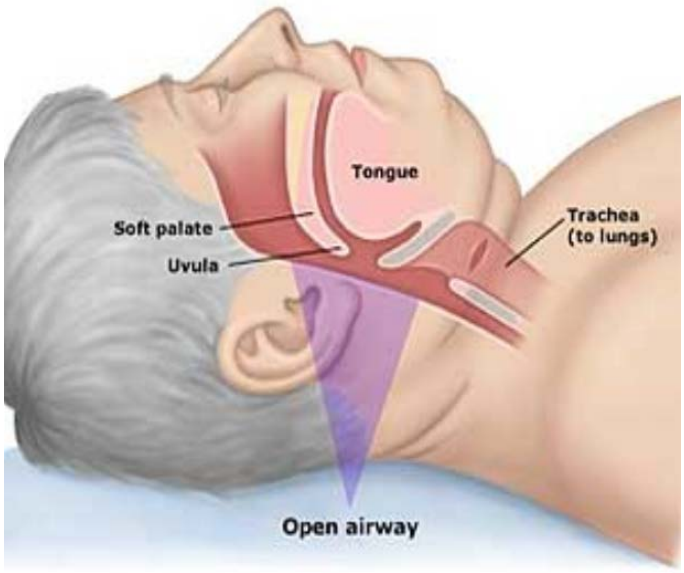

Figure 1.1 Obstructed patient airway [5]

Snoring and sleep apneas often occur together which are caused by changes in patient's upper airway while they go to sleep. The airway may narrow, limiting airflow as patient breathe, which may vibrate, commonly heard as snoring, or it may collapse, so patient stop breathing.

1.2 Obstructive sleep apnea syndrome treatment

There are several methods available for OSAS treatment. This includes surgical treatment to open up an alternative air path through the windpipe or remove soft tissue from the throat; the use of dental appliance to reposition the jaw and tongue; and the use of air pressure (CPAP therapy) to hold the airway open **[7-9]**.

1.2.1 Surgery treatment

Surgery to remedy OSAS is normally done in young patients or those who cannot tolerate using any of the non-invasive forms of treatments. Uvulopalatopharyngoplasty (UPPP) involves the removal of parts of the uvula, soft palate and any other redundant soft tissue including the tonsils, if believed necessary. This procedure often eliminate snoring, however, it may not always treat OSAS since other parts of the airway may be causing the obstruction. Laser-assisted uvuloplataoplasty (LAUP) has become more popular than UPPP since it allows the surgery to be progressively completed over several sessions at a doctor's surgery, eliminating the need for hospitalisation.

More invasive surgical procedure, such as genioplasty where the tongue is pulled forward, is normally conducted when more conservative forms of OSAS treatment have failed. In extremely severe cases, a tracheotomy, where are air pipe is inserted

directly into the patient’s lower airway, is done.

1.2.2 Oral appliances

Oral appliances provide a cheap and easy alternative to other forms of treatment. Oral appliances can be divided into two main groups:

- The mandibular repositioning devices (MRD), Figure 1.2, is the largest group of oral treatment devices, which operate by tightening the patient's teeth and pulling the bottom jaw forward into a "bulldog bite" and holding the teeth in the most closed position possible. The difference in appliances is in the style of adjustment hardware, the position of the adjustment hardware, and the material used in the appliance itself. Some patients will find one appliance more comfortable than the others. There is no one appliance that will work for every patient.

Figure 1. 2 Mandibular repositioning device [10]

- The tongue retaining device (TRD), Figure 1.3, is used in patients suffering from OSA who have very large tongue, no teeth or chronic joint pain, not suited to MRD oral devices. TRD directly holds the tongue in a forward position by means of a suction bulb. When the tongue is in a forward position, the back of the tongue does not collapse during sleep and obstruct the airway in the throat.

Figure 1. 3 Tongue retaining device [11]

- A variation on the TRD, the jaw and tongue retaining device, Figure 1.4, utilise two separate appliance portions, each fitted to the top and bottom row of teeth. It serves to open the airway by indirectly pulling the tongue forward since the tongue is attached to the lower jaw, by stimulating activity of the muscles in the tongue and making it more rigid, and by holding the lower jaw and other structures in a stable position to prevent opening of the mouth.

Figure 1. 4 Jaw and tongue retaining device [12]

1.2.3 The CPAP Therapy

The use of continuous positive airway pressure (CPAP) therapy, where the patient breaths air pressure slightly above atmospheric pressure, effectively prevents collapse or blocking from occurring by forming a pneumatic splint within the patient's breathing airways and is the most common form of OSA treatment, as shown in Figure 1.5 and Figure 1.6. The CPAP system is a small bedside unit that gently boosts the pressure in patient's airway keeping the airway open while patients are asleep. The pressurized air inside of the airway produces the restitution of airflow and is an effective therapy for OSAS in many patients by improving the sleep quality of patients **[13, 14]**. The CPAP was introduced in New Zealand have many years **[15]**, and the original CPAP machine was introduced in 1981 by Australian Dr. Colin Sullivan and his associates. They reversed a vacuum cleaner motor so that it would blow air into a patient's nasal cavity via tubing to keep the passage open. This applies positive air pressure into the upper airway and pushes a constant flow of air into the lungs **[16]**.

1.2.3.1 Component of the CPAP

The CPAP system (as shown in Figure 1.5 and 1.6) consists of an air delivery unit, supplying low pressure air to the nasal mask via a 20mm internal diameter flexible plastic hose. A humidification reservoir is the humidity required by the neonate in the system. Sterile water is fed into the chamber. The water level is controlled by a dual float mechanism, water is utilised between the fan and mask to humidify the breathing air, preventing the patient's airways becoming dry and irritated **[17]**.

The level of air pressure required for CPAP treatment is frequently a trade-off

between being sufficient to prevent obstruction of the airway whilst minimising pressure related side effects. Typical CPAP titration air pressures range from 6 to 20cm water gauge. The prescribed CPAP mask air pressure is determined by nocturnal polysomnography testing of each patient to determine the minimum CPAP titration pressure required to prevent OSA from occurring.

Figure 1. 5 Commercially available CPAP ADU and humidification [17]

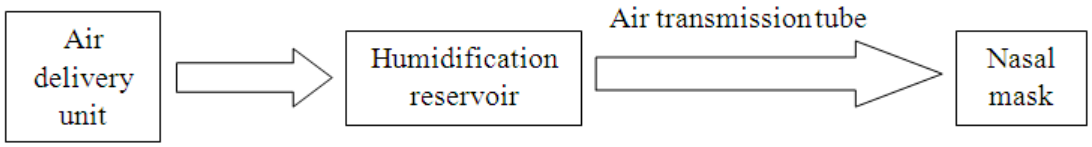

Figure 1. 6 Schematic diagram of CPAP device

The CPAP therapy can be applied to the patient either orally (Oral CPAP), shown in Figure 1.7, or through a nasal mask (Nasal CPAP), shown in Figure 1.8, the latter having the advantage of avoiding drying of the patient's throat due to the continuous airflow. Despite using a nasal mask, some patients develop dry mucus membranes; however, this problem can be reduced by humidification of the air flowing into the mask.

Figure 1. 7 The Oral CPAP [17]

Figure 1. 8 The Nasal CPAP [18]

- The Oral CPAP

The Oral CPAP is an oral mask which delivers pressure exclusively through the mouth rather than the nose. It is small, unobtrusive and easy to wear. The mouthpiece comes in two sizes and is placed behind the lips and in front of the teeth. An outside flap is then fitted into the mouthpiece and folded over the lips. This combination keeps the device stable in the mouth and has been redesigned without the inner flap of the earlier design, which rested on the tongue **[17]**.

- The Nasal CPAP

The Nasal CPAP is a simple, lightweight single-piece mask made of soft medical silicone that provides comfort, durability, and flexibility. It prevents drying of the patient's throat due to the continuous airflow. However, some patients experience dry mucus membranes which requires humidification air to address this problem **[18]**.

Typical mask shown in Figure 1.9 is comfortable and provides a proper seal for the airflow and should be fitted correctly to deliver the proper air pressure level

Figure 1. 9 Typical nasal mask [19]

1.2.4 Improving CPAP system

Many healthcare providers consider patient non-compliance to be the biggest problem with CPAP therapy, usually on patients using the machine only a few hours at sleep time or a few days each week. Despite felt discomfort appearing to be the main cause of treatment failure, patients suffering Snoring or OSA are often more compliant than mild sufferers due to the benefits of treatment success.

Recent research has found, comparing the result of CPAP and the Automatic Positive Air Pressure (APAP) treatment has shown all patients benefited from air pressure therapy. However, variations occurred in the patient's sleep response to either form of treatment. These data results indicated patient compliance improved when lower mean mask pressures were used and suggested that long term studies could quantify the beneficial effects, such as greater comfort and reduction in visceral strain, when mask pressure was reduced.

The aim of the project is maintain mask air pressure within ±0.5 cm Wg of the desired value whilst the patient is breathing by utilizing pressure feedback control of ADU. An idealized the size ranging of the micropump from 0cm to 20cm, it will be simulated to identify various control scenarios **[20-21]**.

There is an opportunity to improve CPAP breathing therapy device. This will be achieved in APAP system with the variable output Air delivery unit (ADU). The new ADU will required to miniaturize and generate more air flow than existing system in order to overcome the additional air flow resistance offered by the small diameter air tube.

1.2.5 Bi-Level positive airway pressure

Bi-level positive airway pressure breathing therapy devices operate in a similar fashion to CPAP devices with the exception of offering two air output pressure levels from the ADU.

The Bi-level positive airway pressure incorporates a "sensing feature that helps determine and vary the suitable pressure depending on whether a person is breathing in or out." In this case, upon inhaling a patient receives more pressure and when they exhale they receive less. **[22]**.

Bi-level positive airway pressure system is most advantageous to patients who either have tremendous amounts of carbon dioxide in their systems or those who already have pre-existing lung disease.

1.2.6 Automatic positive airway pressure

The Automatic positive air pressure (APAP) system is the most sophisticated CPAP device available. This device senses nasal mask pressure and appropriate control action is taken by the air delivery unit (ADU) by altering the fan speed. This enables mask pressure to be progressively reduced during periods of absences of apneic events.

These devices can work in one of three ways:

Firstly, the pressure of the machine can be kept to a low level until the patient experiences problems breathing. Once that happens, the pressure can then be dramatically increased.

Secondly, the pressure can be kept low and steady until a problem arises at which time it is raised in a steady way.

Thirdly, the pressure of the machine can be put up or down according to breathing problems. It can also detect when there is a problem developing in between “single breaths” of the patient **[23]**.

Unlike other forms of air pressure therapy, APAP treatment is intended to continuously take corrective action over a period of time and offers the advantage, over conventional CPAP therapy, of reduced adverse pressure elated side effects due to lower average mask air pressure. It does not, however, offer any remedy for fluctuations in mask pressure due to the fluctuating patient breathing load.

1.3 Research objective

The objective of this project is to develop and design a miniaturize piezoelectric micropump for Air Delivery Unit (ADU) in the CPAP system. The experimental results in the project are obtained using standard techniques, so that the performance of new concept micropump can be evaluable against or replace other traditional micropump. The micropump design performance specifications will be based on a breathing system model simulation, incorporating on characteristics of gas inertia, effects of fans installation details on fan performance and fluctuating air flow resistances.

The main objectives of the work are:

- Develop suitable flow configuration to provide a miniaturized air flow pump. This including: Design and build the various configurations to achieve the objective of this work.
- Develop a mechanical model to determine characterizes of micropump.
- Develop the fluid model for flow rate and air pressure base on the proposed type of micropump.
- A mathematical model will be developed to optimize the fan and determine its optimum performance.
- Investigation of the oscillatory behaviour interaction, generating flow rate due to the action and reaction principle.
- Development of a prototype, production of micropump performance calibration charts and dynamic behaviour.
- Setup an experimental to conduct testing on the developed pumps.
- Conduct appropriate computing simulations on the fluid flow in the develop system for optimization propose.
- Combine with other elements and test the overall system performance.
- Investigate performances of the proposed mini micropump and give appropriate recommendation for future work.

1.4 Thesis structure

Characterizes of Piezofans is presented in Chapter 2, it is used for analysis and design of micropump. Chapter 3 and 4 is described the experimental setup and experimental results, using experimental results and theoretical analysis the maximum air flows and air pressures. Chapter 5 and 6 will have some conclusions and future design for the micropump.

Chapter 2 Piezoelectric Fan

2.1 Introduction

This chapter given the scientific and engineering background for piezoelectrically fans, some introductory materials on piezoelectricity fan developed at operation and performance are elaborate on.

2.1.1 Micropump technology review

Most micropumps found today can roughly be divided into two large groups: “displacement micropumps” and “dynamic micropumps”. The first group is includes the so-called “reciprocating micropumps”, that uses the oscillatory or rotational movement of mechanical parts to displace fluid, the most known of which are the diaphragm micropumps. In the other group is includes electro-hydrodynamics, electro-osmotic, magneto-hydrodynamics, acoustic streaming, ultrasonic and other types of micropumps. Reciprocating micropumps are generally suitable for the delivery of all gaseous and lower viscosity fluids, and most dynamics micropumps depended on certain properties of the fluid such as ionic strength. Several principles, such piezoelectric, electrostatics, and thermal actuation have been adopted to develop micropumps. Many of new concept micropumps development are based on the use of piezoelectric actuators that have simple structure, low noise generation, small in dimension, high efficiency output, lower power consumption and long lifetime. According to these features, the piezoelectric micropumps are suitable to reduce the size of the Air Delivery Unit (ADU) in the Positive Airway Pressure System (PAPS). As these pumps delivery small amount of air and pressure, valve-less system is more practical to avoid the friction and loosen association with normal mechanical valve.

2.1.1.1 Valve-less piezoelectric micropumps

Valve-less piezoelectric micropumps belong to the diaphragm micropump, similar to a piston. It is use a piezoelectric actuator to move a piezoelectric membrane in a chamber providing fluid entrance and exit with the flow direction being controlled by check diffusers / nozzle.

This micropump is one of the most promising devices for a new concept of medical care technology, shown in Figure 2.1. The proposed micropump is designed for fluid with high viscosity such as blood and hence it can easily be adapted to other fluids. The most important characteristic of the pump is the double superimposed chamber, where the upper and lower chambers share the same membrane in a “sandwich” type of form.

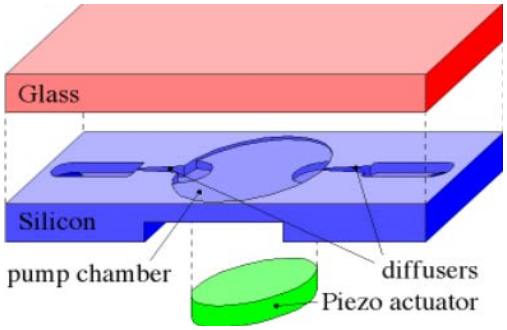

Figure 2. 1 Valve-less micropump [24]

Because piezoelectrically actuated valve-less micropumps have simple structure and no internal moving, there is less risk of clogging the valves when it pumps fluid containing particles. Also, they can respond more quickly than other kinds of micropumps. However, valve-less micropumps need higher actuation supply voltage, generate higher noise, lower flow rate output and easily to breakdown inside the capacitor (piezoelectric material). Therefore, another type of actuating piezoelectric fan micropumps also have been widely used and designed.

2.1.1.2 Actuating piezoelectric fan micropumps

Actuating piezoelectric fan micropumps are important instruments in areas such as biology and medicine. The micropump device, which composed of a rectangular piezoelectric fan and a closed chamber, and two check valves, can delivery gas or liquid in one direction, the simple micropump as shown in Figure 2.2.

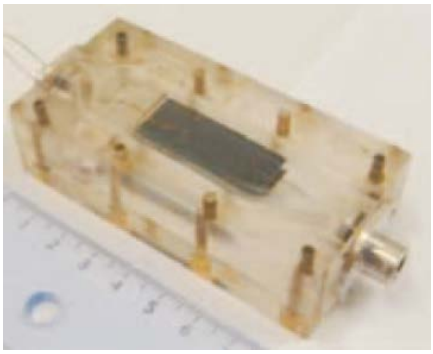

Figure 2. 2 Actuating piezoelectric fan micropump [25]

The single piezoelectric fan to generate the oscillation, such this motion will produce higher flow rate to pump gases to the output. Therefore, innovative this micropump are also investigated as alternative replace traditional Air delivery Unit (ADU) in small scale where increasing the value of its efficiency and useful.

2.2 Basic piezoelectric fan

Piezoelectric fans are cantilever beams which are fabricated by bonding a piezoelectric patch or several patches to a shim material made of Mylar or metal and cut to a desired shape and size. When an alternating voltage is applied to the piezoelectric patch, it expands and contracts in the lengthwise direction at the frequency of the input **[31]**. This applies bending moments at the beginning and end of the piezoelectric patch effectively. As the input signal frequency approaches the fundamental resonance frequency, large vibrations occur at the cantilever tip, as

shown in Figure 2.3. This oscillatory motion generates air flow and pressure that can be exploited for cooling or delivering air flow **[32]**.

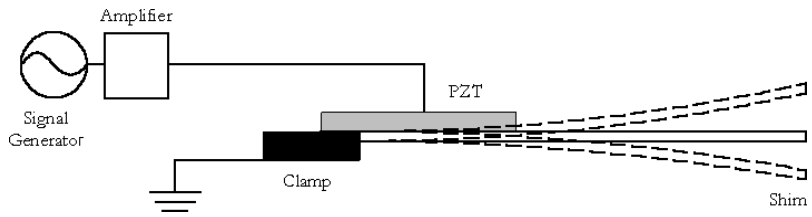

Figure 2. 3 Schematic of piezoelectric fan

2.2.1 The piezoelectric fan properties

A piezoelectric fan is a composite electromechanical structure that converts electrical potential into mechanical strain. The piezoelectric fan used in this research is a commercially available piezoelectric actuator bonded to flexible cantilever beam (Mylar) **[37]**, from Piezo System, INC (USA). The oscillating Mylar blade is driven at resonance frequency by a piezoelectric bending element. In free air, the maximum amplitude resonance vibration of the Mylar blade causes the formation of a high velocity unidirectional flow stream. Maximum air flow and air pressure occur along the axes of the fan's centerline. A simple equivalent electrical circuit model of the piezoelectric fan shown in Figure 2.4. The resistor R_1 represents the irreversible leakage of electrical energy into electrical and mechanical dissipation, the inductor L_1 represents the mass of the oscillator, and the capacitor C_1 is represents the storage of strain energy in the structure. The capacitor C_0 corresponds to the capacitance of the piezoelectric ceramic path and represents the electrical energy stored **[38]**.

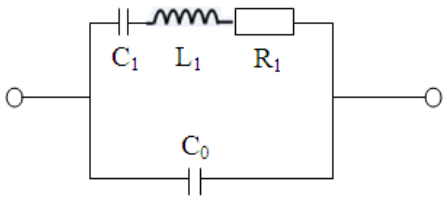

Figure 2. 4 Equivalent circuit diagrams for a piezoelectric fan

Such above circuit have two natural frequencies, maximum and minimum frequency, namely f_m and f_n. The electrical energy can be converted to mechanical energy in such an electromechanical system. The dynamic electromechanical coupling factor (EMCF) of the circuit **[39]**

$$EMCF = \sqrt{\left(\frac{f_n^2 - f_m^2}{f_n^2}\right)} \quad (2.1)$$

The maximum frequency f_m represents the short circuit series resonance frequency of the R-L-C branch, whereas f_n represents the open circuit resonance frequency of the complete circuit.

2.2.2 The resonance frequency of piezoelectric fan

The accurate calculation and measurement of the short and open circuit resonance frequencies and mode shapes of a piezoelectric fan are important for several reasons. First, when the circuit is shorted, when the piezoelectric fan is driven at resonance frequency, the equivalent circuit impedance is minimized locally, resulting in greater mechanical energy or maximum amplitudes of fan vibration. Second, the difference between the open and short circuit resonance frequencies provides a measure of mechanical oscillation of the fan. Third, the prediction of mode shape itself is important, because it is directly correlated to the flow field surrounding the fan **[40]**.

The resonance frequency of the piezoelectric fan can be determined by three methods:

A. Measuring the impedance of the piezoelectric fan circuit as a function of frequency.
B. Using finite element analysis to predict the resonance frequency based on electromechanically characteristics.
C. Qualitative observation of the flow produced by the fan to determine the

frequency at which maximum flow is achieved **[41]**.

2.2.3 Power consumption and losses of piezoelectric fan

Power consumption is a critical issue that can enhance or nullify any advantages to operating at the piezoelectric fan resonance modes. The following equation is calculating for the power consumption of the piezoelectric fan:

$$P = \frac{1}{t}\int_0^t v(t')i(t')dt \tag{2.2}$$

Where ***t*** is the time period over which the signal is measured, ***v*** is the input voltage and ***i*** is the current to the piezoelectric fan can be determined by 1KΩ resistor connected by series between the piezoelectric fan and ground, and measuring the voltage drop between the power supply and ground, and across the resistor **[42]**, as Figure 2.5 shown.

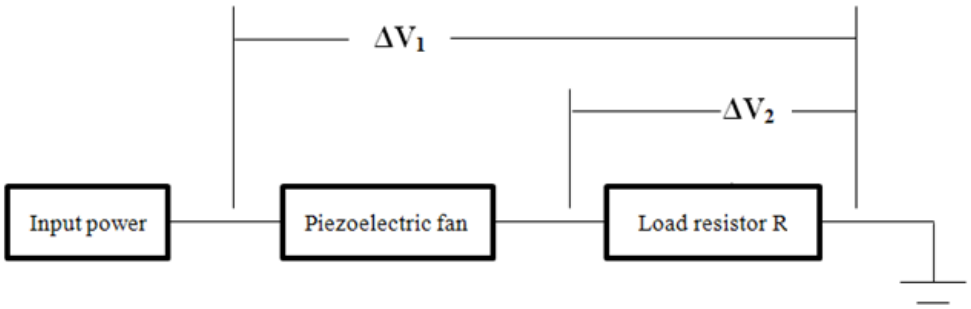

Figure 2. 5 Diagram of power consumption measurement

The time varying input voltage, ***v (t')*** is measured as ΔV_1 and time varying current, ***i (t')*** is measured as $\Delta V_2 / R$ using a digital oscilloscope.

Piezoelectric losses exist with mechanical dielectric at the same time. The equivalent circuit with resistance ***R***, inductance ***L*** and parallel capacitance C_0, C_1 values representing the dissipation, inertial and storage terms for the system. The resistance

contributes to the resistive or the real part of the equivalent circuit impedance, while the inductance and capacitance contribute to the reactive or imaginary part. The series impedance, ***Zs*** is given by the following equation:

$$Zs = R + j\omega L + 1/j\omega C \tag{2.3}$$

And the total impedance, ***Zt*** is given by:

$$Z_t = \frac{Z_S(\frac{1}{j\omega C_0})}{Z_{S+}(\frac{1}{j\omega C_0})} \tag{2.4}$$

The total loss in the system is quantified as the tangent of the angle between the imaginary axis and the magnitude of the impedance, as shown in Figure 2.6. While that ***tan α*** is zero, the impedance is purely reactive (no energy loss), and the larger angle α is the greater the loss in the system **[43]**.

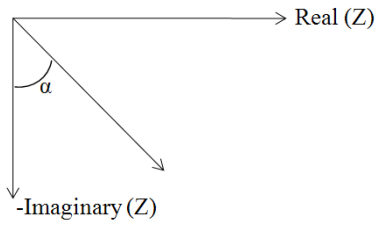

Figure 2. 6 Schematic illustration of impedance in the real and imaginary plane

2.2.4 Theoretical analysis of the piezoelectric fan

Because a piezoelectric fan is fabricated by bonding a piezoelectric patch and a Mylar blade, the oscillating Mylar blade is driven at resonance by the piezoelectric patch. Thus, the whole system of piezoelectric fan can be simplified into a two-degree vibration of freedom for modal analysis. When the piezoelectric fan is driven by the resonance frequency, the air flow is actuated by the piezoelectric device in the pump chamber. The general equation of the actuating part on the pump chamber, which is

shown in Figure 2.7, can be express as equation **[44]**:

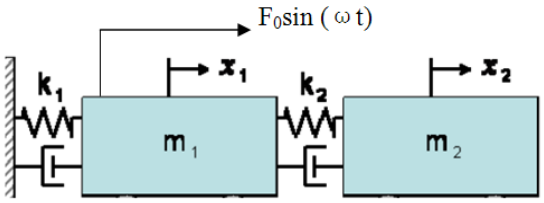

Figure 2. 7 Schematic of a vibration absorber with damping in both the primary and absorber system [45]

$$F_0 sin(\omega t\ ) = Mx'' + Cx' + Kx \quad (2.5)$$

$$\omega = 2\pi f \quad (2.6)$$

In the left-hand term, $\boldsymbol{F_0 sin\ (2\pi ft)}$ represents a force due to the input voltage; f is the input frequency of the input AC sine waves. $\boldsymbol{M}$ is represents the total equivalent masses of the piezoelectric device; $\boldsymbol{C}$ is the total equivalent damping coefficient of the piezoelectric device; $\boldsymbol{K}$ is the total equivalent spring constant of the piezoelectric device; x'' is the vibration acceleration of device, x' is the vibration velocity of the device; the x is vibration amplitude of the device.

The coordinates that completely describe the motion of this system are $\boldsymbol{x_1(t)}$ and $\boldsymbol{x_2(t)}$, measured from the equilibrium position of each mass and an external force $\boldsymbol{F_0 sin\ (\omega t)}$ act on mass $\boldsymbol{m_1}$. Using Newton's second law, the free body diagrams showing forces acting on each mass is shown in Figure 2.8.

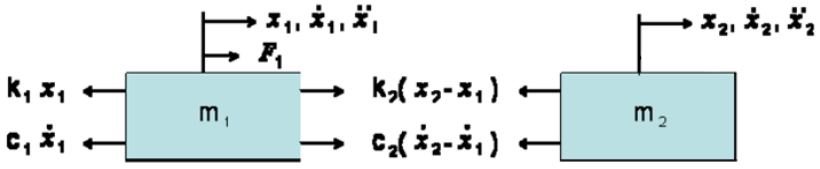

Figure 2. 8 The force analysis [45]

From these free body diagrams the equations of motion are easily found:

$$m_1 x_1'' + (C_1 + C_2)\, x_1' - C_2\, x_2' + (k_1 + k_2)\, x_1 - k_2 x_2 = F_1 \quad (2.7)$$

$$m_2 x_2'' - C_2 x_1' + C_2 x_2' - k_2 x_1 - k_2 x_2 = 0 \quad (2.8)$$

The equation of the motion can put into matrix form:

$$[m] = \begin{bmatrix} m_1 & 0 \\ 0 & m_2 \end{bmatrix} \; [c] = \begin{bmatrix} -c_1 + c_2 & -c_2 \\ -c_2 & c_2 \end{bmatrix} \; [k] = \begin{bmatrix} k_1 + k_2 & -k_2 \\ -k_2 & k_2 \end{bmatrix} \; \{x\}$$

$$= \begin{Bmatrix} x_1 \\ x_2 \end{Bmatrix} \quad \{F\} = \begin{Bmatrix} F_1 \\ F_2 \end{Bmatrix}$$

$$\begin{bmatrix} m_1 & 0 \\ 0 & m_2 \end{bmatrix} \begin{bmatrix} x_1'' \\ x_2'' \end{bmatrix} + \begin{bmatrix} -c_1 + c_2 & -c_2 \\ -c_2 & c_2 \end{bmatrix} \begin{bmatrix} x_1' \\ x_2' \end{bmatrix} + \begin{bmatrix} k_1 + k_2 & -k_2 \\ -k_2 & k_2 \end{bmatrix} \begin{bmatrix} x_1 \\ x_2 \end{bmatrix} = \begin{bmatrix} F_0 \\ 0 \end{bmatrix} sin\omega t \tag{2.9}$$

Chapter 3 Experimental Setup

3.1 Introduction

This chapter presents the design configurations which were developed during the course of this research to test the concept of piezoelectric. The proposed configurations are discussed and tested to determine their performance characterization.

3.2 Single piezoelectric fan analysis

Before developing an appropriate pump configuration, an investigation was conducted to determine the performance of the piezoelectric fans used in investigation. A piezoelectric device is characterized by generating a force or vibration when a voltage is applied, and also generating a voltage when a force is applied.

The vibration of the fan found in this harmonic analysis can be prescribed in a fluid flow simulation as an approximated way to reproduce the behavior of the pump system without the need of a complete analysis considering both piezoelectric effects and fluid system, which could be computationally heavy.

The piezoelectric fans used in this project are commercial products with piezoceramic bonded to a flexible cantilever beam (Mylar). The input voltage and frequency are tuned to the first resonance frequency of the blade to provide large oscillations.

A typical piezoelectric fan is shown in Figure 3.1. In this diagram, the footprint of device is described by the overall fan length (Lo) and fan width (D). Because the oscillating Mylar blade (Flexible blade) is driven at resonance by a piezoelectric bending element, the largest oscillations occur within the portion of the flexible blade not covered by the piezoelectric material. Therefore, the exposed Mylar blade length

(L) is also important in this device.

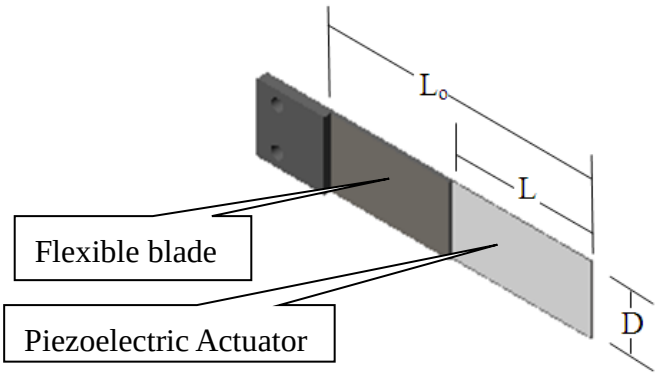

Figure 3. 1 A typical piezoelectric fan

The piezoelectric fans used in this project have a Mylar blade bonded under a few piezoelectric layers (in parallel connected). Thus, when the electric energy converts into mechanical energy, the Mylar blade is deformed proportionally to the applied load, creating a large oscillatory movement. The piezoelectric fan used in the project has 76.7mm total length (include 32.0mm length of piezoelectric layers, 64.0 mm Mylar and 12.7mm length of PCB board), 12.7mm width, 0.53mm thickness of piezoelectric material and 0.25mm thickness of Mylar blade. The maximum amplitude is 25.4mm; capacitance is 15nF and 2.8 g weight.

To better understand the behavior of the piezoelectric fan, its application in the micropump, and also to generate input data for fluid simulations, an analysis of the piezoelectric fan in fluid environment is conducted **[52]**. Firstly, harmonic analysis is carried out to obtain electrical impedance and resonance frequency of the piezoelectric fan in air. An experiment was conducted to define the characterization of a single fan in a closed channel as shown in Figure 3.2. This model shows the side view of the piezoelectric fan where ***A*** is the amplitude of oscillation at the tip of the piezoelectric fan and the frequency of oscillation, respectively.

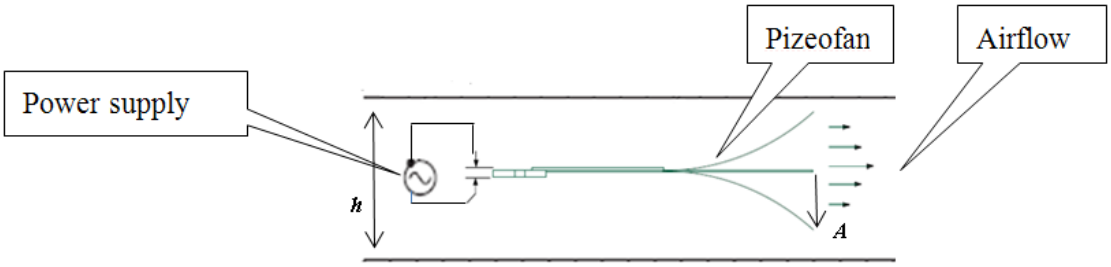

Figure 3. 2 A piezoelectric micro pump scheme

"h" represents the width of chamber is equal to 6.1 cm. The resonance frequency mode, considering the fluid environment around the actuator has a frequency of 60 Hz with maximum amplitude (***A***) at the tip of the piezoelectric fan of 2.54 cm for applied voltage of 115Vpp. The chamber width and its length are long enough and airtight to avoid the influence of pressure boundary condition. The flow meter (WaveFront Flow Meter D-22) is used to produce the flow characterization, to find out the general relationship between flow rate and pressure is readily observed by normalized each time with its respected maximum values.

In this project, another one important issue to match computational and experimental values is the damping ratio of the piezoelectric fan (including piezoelectric blade and Mylar blade) which is unknown **[53]**. Thus, a calibration procedure is necessary and adopted as follows. An experimental Logarithmic decrement, δ is measured with a Vibrometer controller (Polytec OFV-5000), which is used to find the damping ratio of an under damped system in the project. Once the damping ratio of piezoelectric blade and Mylar blade are found, these same values are adopted to find the real resonance frequency, and compare with the data sheet to prove the final conclusion (Appendix A).

3.3 Single piezoelectric micropump configurations

The micropump with a piezoelectric device is driven by an alternative sine wave generator. The input signal within ±115 V at 50 ~ 70 Hz is controlled by an AC power supply. The single piezoelectric micropump flow rate data are recorded to analyze the pump performance under a different input voltage and frequency.

The principle of pumping proposed in this project mimics a phenomenon commonly seen in nature: the swimming fish motion. This phenomenon has been widely studied. When fishes swim, most of them have propulsion generated by moving their bodies and tails. In this area, fishes exhibit oscillatory motion, shaking their bodies and tails, moving forward without a propagating wave formation, as shown in Figure 3.3 **[55]**.

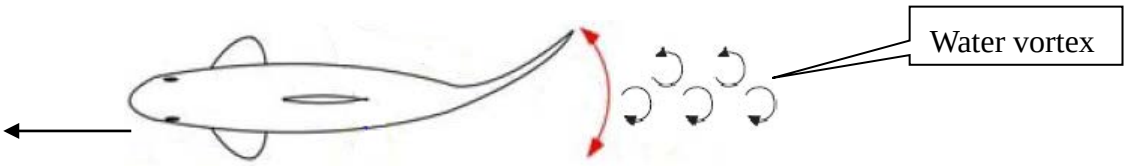

Figure 3. 3 Formation of a vortex street

The fish makes an oscillatory motion, moving itself forward. A fluid motion will be observed, therefore the fish swimming as a flow pump. This phenomenon is similar to a thin plate in oscillatory motion inside a fluid environment. In this project, vortex generation is obtained by oscillating piezoelectric actuator, which yields fluid motion inside the micropump, as shown in Figure 3.4.

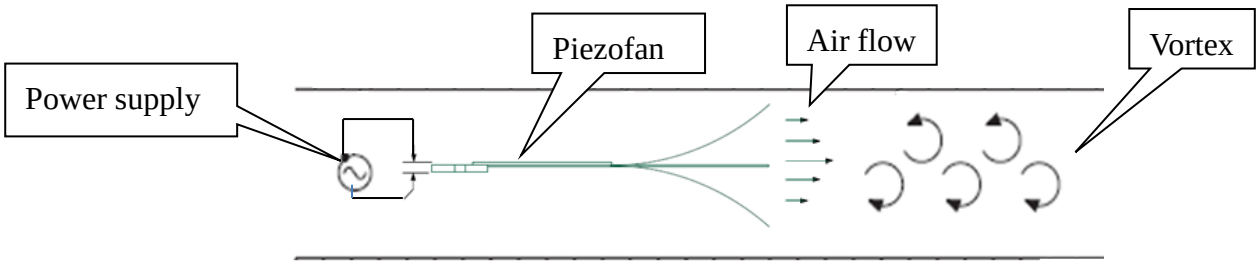

Figure 3. 4 A piezoelectric pump scheme

3.4 Experimental procedure set-up

3.4.1 Experimental procedure for single piezoelectric fan

An air chamber was designed as detailed in Appendix B. The experimental instruments used to measure the air flow rate and air pressure characteristics consist of a few airtight chambers with single piezoelectric fan or two piezoelectric fans in series or parallel configurations **[56]**. A schematic diagram of the experimental setup is shown in Figure 3.5, in which the piezoelectric fan under investigation is positioned to direct air flow inside the airtight chamber. The static air pressure generated by the fan (P) is measured with a pressure transducer (Novasina Pascal Switch 100 with accuracy ± 0.25 Pa). The flow rate (Q) is determined by flow meter (Wave Front Flow Meter accuracy ± 0.5 L/min).

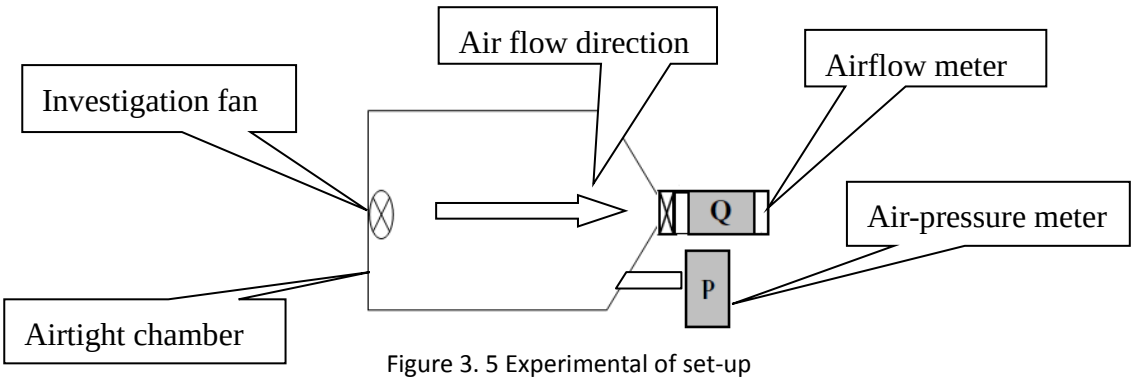

Figure 3. 5 Experimental of set-up

The measurement process begins by closing the channel to capture the attainable pressure at a zero flow rate condition (P_0). Next, the valve was opened and we waited for the static pressure (P) in the chamber to reach zero. In this moment, the flow rate is attainable at a zero pressure condition (Q_0). Each new setting represents a point along the pressure-air flow rate curve which starts at P_0 and Q_0.

A micropump prototype is built for validation purposes. In this section, experimental methods and materials used for the prototype characterization are described.

Moreover, results obtained for the performed experimental tests using the piezoelectric micropump prototype will be presented.

The micropump prototype is shown in Figure 3.6. It is composed by one or two piezoelectric actuator (in this section, only used one actuator is used), which has a total length of 17.1cm, width 10.1cm and 1.6 cm deep channel, composed by three parts top, bottom are symmetrical and the middle part, made of acrylic, and inlet and outlet connector, of 1.3 cm diameter, which are made of aluminum. A sequence of an experimental test made for the prototype whose piezoelectric actuator has the aspect ratio of 7.7cm×1.27cm. The experiments were conducted at ambient temperature. The prototype is driven by an AV power generator (Titan AC power system); applied 115Vpp with an excitation frequency ranging from 50Hz~70Hz and it has a duct height of 1.5cm, as previously mentioned in above section.

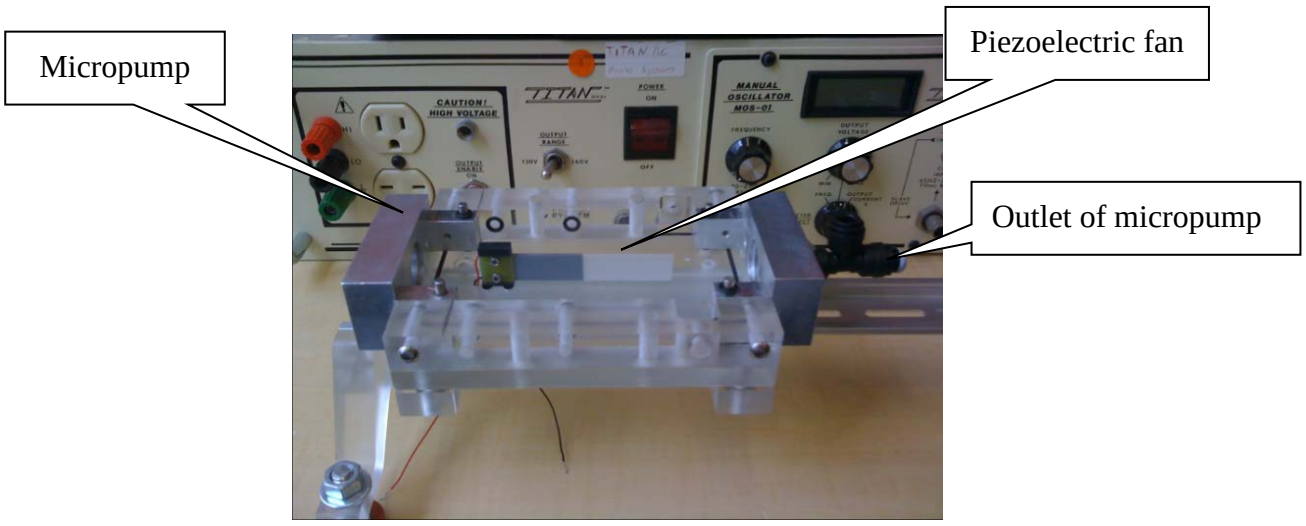

Figure 3. 6 The prototype of micropump

The experimental setup used in the simulations is shown in Figure 3.7 and 3.8. The setup consists of connecting a plastic tube, with known length and dimension of hole, in series connected with the micropump outlet.

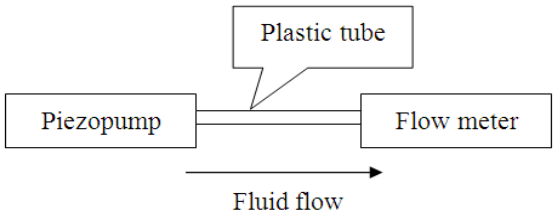

Figure 3. 7 Experimental flow rate characterization scheme

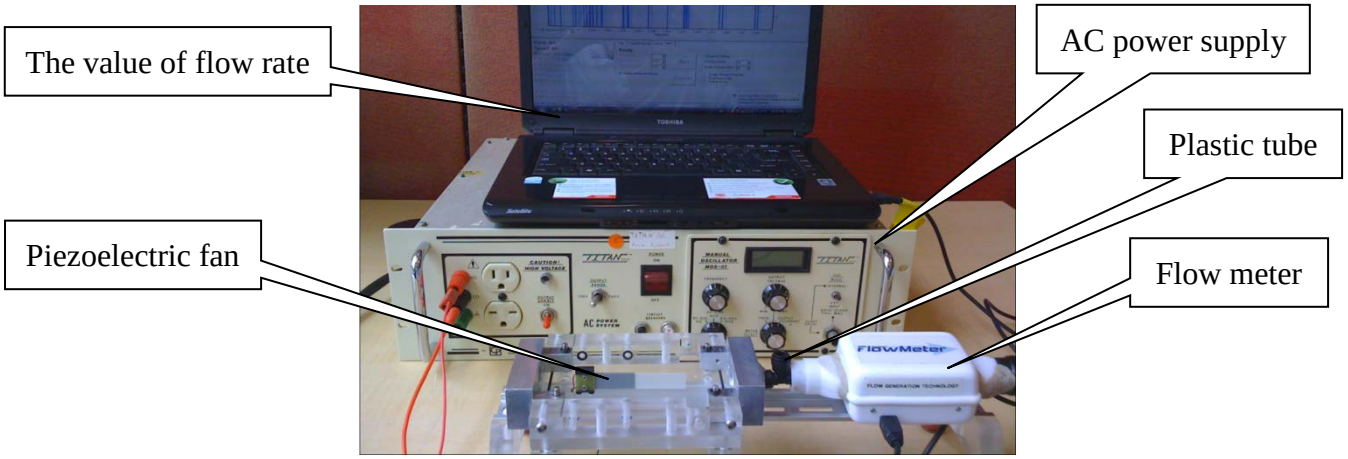

Figure 3. 8 The experimental setup

3.4.2 Parallel-series configurations

As the previous sections mentioned, the oscillatory behavior yields vortex interaction, generating flow rate due to the action and reaction principle. Thus, following this idea the objective of this section is to investigate this oscillatory principle by studying the interaction among generated vortex from two piezoelectric fans oscillating inside the same chamber, which is similar to the interaction of vortex generated by right, left or frontal, posterior fish when they swim together in a group formation. The main objective is to deliver which fan configurations gives better performance **[57]**. The configurations are show in Figure 3.9, and they will be investigated **[58]**

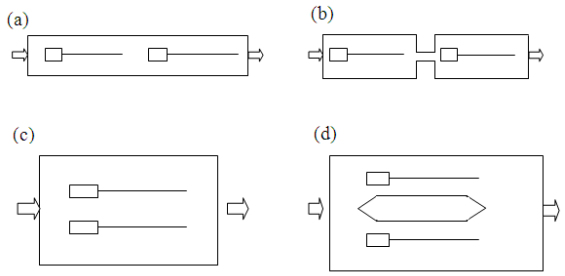

Figure 3. 9(a) Two fans in series configuration, (b) two single pumps connected in cascade, (c) two fans in parallel configuration, (d) two single pumps connected parallel.

3.4.2.1 Pump configurations

Experimental prototypes of both cases (parallel and series configuration) are built to investigate the performance of the pump. Results obtained from the experimental tests using these pump prototypes are presented in this section.

Figure 3.10 and Figure 3.11 show the experimental models which are built considering two piezofans in parallel and in series configuration, respectively. The pump prototype for parallel configuration is composed by two piezofans allocated inside a channel constructed in a pair of symmetrical parts, made of acrylic, and which has 17 cm length. In the prototype for series configuration two piezofans are positioned in a channel which has 13.5 cm length. In both cases the channel has 21 ~ 66 cm^2 transversal section, and the piezofan has a total length of 7.67cm each. Moreover, these prototypes have a pair of rectangle inlet and outlet connectors.

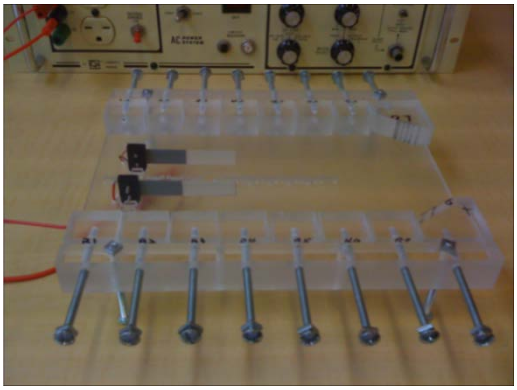

Figure 3. 10 Pump prototype with parallel configuration

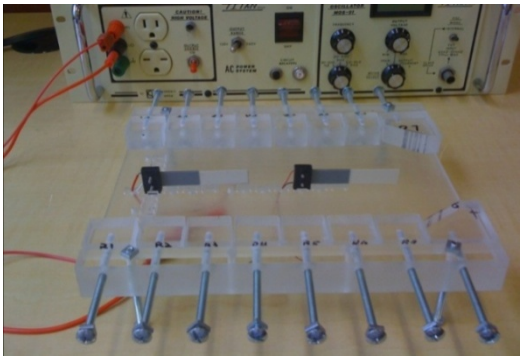

Figure 3. 11 Pump prototype with series configuration

According to the description of the above section, as in figure 3.12 and Figure 3.13 shown the dimensional characteristic of model applied to simulate two piezoelectric fans in parallel and series configurations **[59]**.

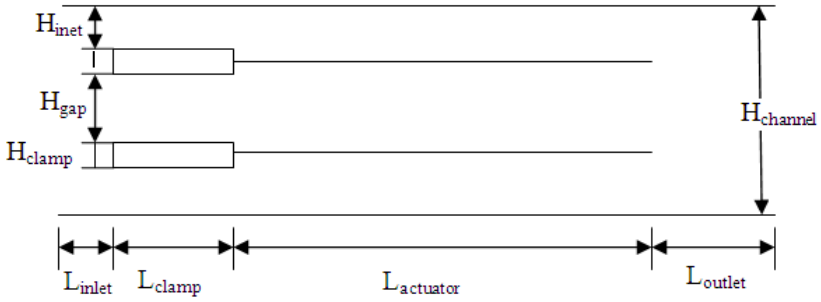

Figure 3. 12 Two piezoelectric fans in parallel configuration

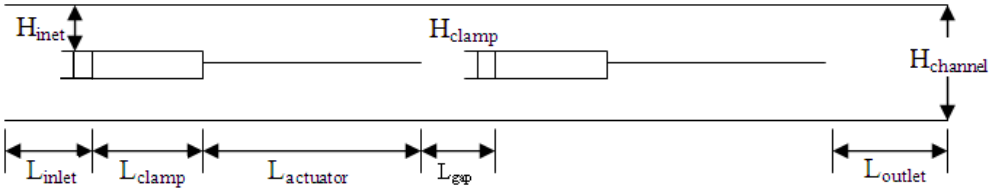

Figure 3. 13 Two piezoelectric fans in series configuration

A sensitivity analysis is carried out to obtain the optimum values for inlet dimension ($\boldsymbol{H_{inlet}}$), distance between two parallel piezoelectric fans ($\boldsymbol{H_{gap}}$), and distance between two series fans ($\boldsymbol{L_{gap}}$).

In parallel configuration model depicted in Figure 3.25, $\boldsymbol{H_{inlet}}$ and $\boldsymbol{H_{gap}}$ values must satisfy $\boldsymbol{2H_{inlet} + H_{gap} + 2H_{clamp} = H_{channel}}$, where $\boldsymbol{H_{channel}}$ and $\boldsymbol{H_{clamp}}$ are equal to

1.7cm and 1 cm, respectively. Initially, the dimensions 2; 3.5; 5; 6.5; 8 and 9cm are specified for $\boldsymbol{H_{gap}}$, and then $\boldsymbol{H_{inlet}}$ is specified from 1~4.5 cm, respectively. Thus, a total of 12 combination values for the pair $\boldsymbol{H_{gap}}$ and $\boldsymbol{H_{inlet}}$ are simulated. In series configuration, the channel has 1.7cm height ($\boldsymbol{H_{channel}}$) and thickness of clamps ($\boldsymbol{H_{clamp}}$) is 1cm. The dimensions 2; 3.5; 5; 6.5; 8 and 9.5 cm are adopted for $\boldsymbol{L_{gap}}$ for performing analysis.

A harmonic motion analysis is carried out to obtain electrical impedance and resonance frequencies of the piezoelectric fans, considering air as fluid medium. Pervious experimental results using a single pump have shown the best performance of the piezoelectric fan occurs when it vibrates in its resonance frequency. It seems to be a good trade-off for the relation between amplitude of vibration vs. input frequencies and air flow rate vs. input frequency.

Experimental pump prototype shows that results obtained considering series configurations of two bimorph piezofans existed with same phase and opposite phase are similar. However, parallel configuration of two bimorph piezofans existed with same phase; (Figure 3.14 (a)) yields better results than existed with opposite phase (Figure 3.14 (b)) due to vortex interaction behaviour illustrated in Figure 3.15. It is noticed that vortex formation occurs at the tip of the piezofans, mutual effects of vortex generated by the two piezofans (in parallel) occur predominantly, contributing strongly for flow rate generation. When excited with phase, two piezofans in parallel configuration generate intercalated vortex streets, as shown in Figure 3.15 (a). However, when excited with opposite phase, aligned vortex streets are generated (see Figure 3.15 (b)), yielding a small flow rate. In addition, when actuators are excited in opposite phase, there is an opposite pressure generation that it may also be responsible for the flow rate decrease. Thus, series and parallel configurations of two bimorph

piezofans excited with phase will be considered in this work.

Figure 3. 14 The vibration mode in air environment (a) same phase (b) opposite phase [59]

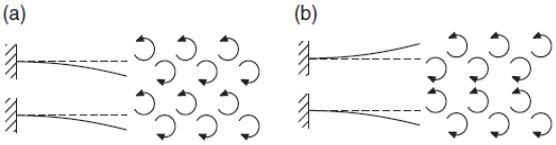

Figure 3. 15 Vortex generation of two piezofans in parallel configuration (a) excited with phase (b) excited with opposite phase [59]

3.4.3 Experimental procedure for double piezoelectric fan with open angle in parallel configuration

The idealised micropump will provide 60 ~ 90 L/min air flow rate and at least of 200 ~ 2000 Pa air-pressures to deliver droplets and air into nasal mask. However, the single prototype could not reach the idealised results. Therefore, it needs to be replaced by new prototype, which is more powerful and more efficient. Subsequent testing of the model, to verify that design is capable of meeting the flow rate and air-pressure requirements of the prototype system.

In this section the performance characteristics of the new piezofans (Quadrature piezofans) and the micropump are determined and assessed against the requirements predicted by the model simulation.

Two counter-oscillating Mylar blade are driven at resonance by two piezoelectric bending elements (Figure 3.16). They move in quadrature, with their trailing edges lagging their leading edges by ninety degrees of phase angle. Each time a blade reverses its motion, it sheds a vortex of air which is rotating too rapid to follow the

blade, and exits at the tip of two blades as shown in Figure 3.17.

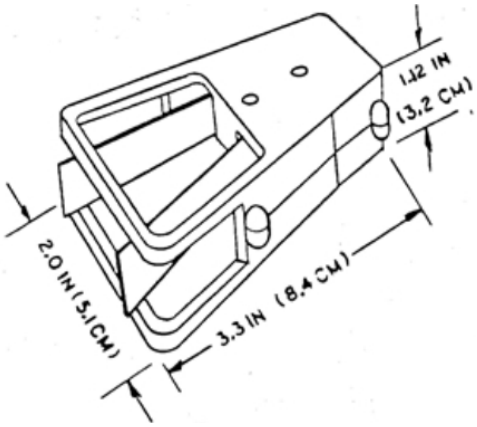

Figure 3. 16 A typical two counter-oscillating Mylar blade.

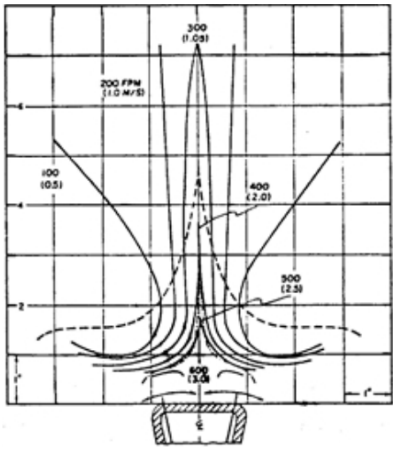

Figure 3. 17 A vortex of air

A schematic representation of the experimental setup used to determine the new micropump prototype characteristics is shown in Figure 3.18 consists an flow meter and an Pascal Switch, and driven by a AC Power supply.

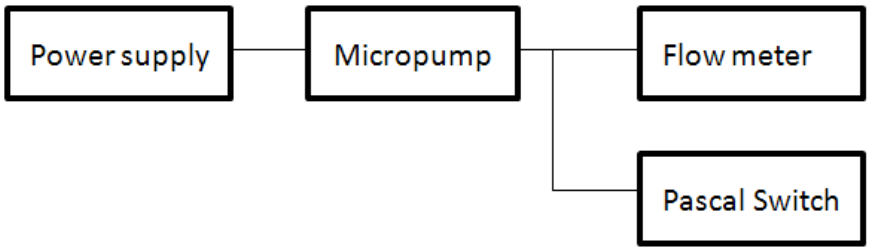

Figure 3. 18 The schematic diagram of experimental setup

The experimental procedure consisted of operating the micropump at stable input AC power supply (115V). The frequency of the AC power input into the micropump was varied from 50 to 75Hz in 1 Hz intervals. The air flow rate from the micropump was adjusting by connecting a soft tube to the exit vent of the micropump, the other end of the soft tube was in turn connected to the flow meter and air-pressure sensor (Novasina Pascal Switch 1000) recorded data during each pressure increment or decrement as diagram shown in Figure 3.19.

Figure 3. 19 The experimental setup

3.5 Summary

A study of configurations of actuators piezoelectric micropump is presented. In the previous work, the obtained maximum flow rate is two piezoelectric fans in parallel configuration existed with same phase, and the maximum air pressure is two piezoelectric fans with same phase in series configuration. Moreover, the improvement of double piezoelectric fan with open angle in parallel configuration is working well. The obtained result is much better than before, the higher flow rate generated by the center of double piezoelectric fan, because the open angle has more powerful strength to push air flow forward. However, the new double piezoelectric fan is still not provide enough air pressure, according to the results, the maximum air pressure achieved by connected two piezoelectric fans in series configuration, therefore, by assembling more double piezoelectric fan inside at same pump channel is advantageous.

Chapter 4 Experimental Results

4.1 Introduction

In the previous chapter presented analysis and investigation of micropump in difference configurations based on placing one or more piezoelectric fans actuator to generate air flow. Experiments set up were performed and their results will be presented in the sequence as objective given in the previous chapter.

4.2 Preliminary investigation-results

The following figures are the results obtained after the calculating and measuring, the relationships between an applied voltage and electric field (Q = CV) as shown in Figure 4.1. The range of input voltage at 0 to 120V, as input voltage raises, increasing the power and generating a situation with maximum peak to peak displacements at the tip of the piezoelectric fan, then resonance oscillating occurs **[60]**.

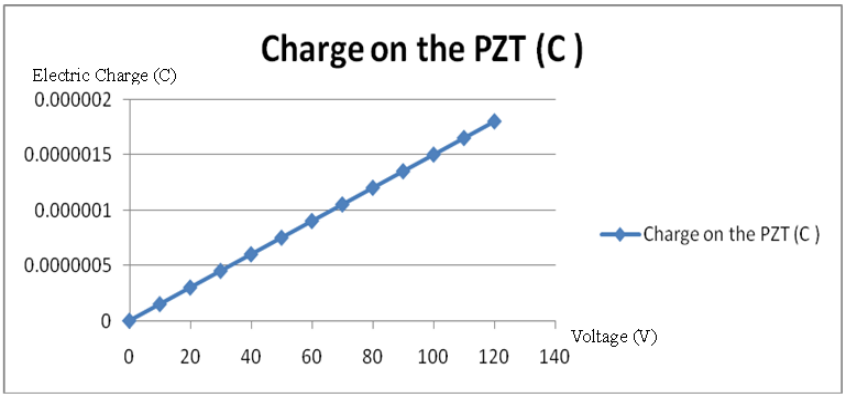

Figure 4. 1 Calculated the electric charge of piezoelectric fan

According to the data sheet of the piezoelectric fan, the maximum vibration occurs at minimum impedance of the actuator in frequency 60Hz, where the maximum amplitude of the oscillation is found, see Figure 4.2.

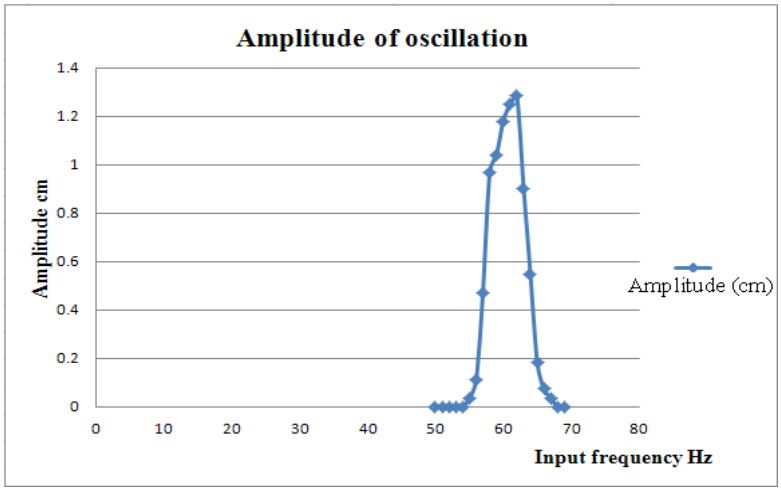

Figure 4. 2 Measured amplitude of oscillation at the tip of the piezoelectric fan

4.3 The single piezoelectric fan testing results

Firstly, the flow rate (L/min) versus frequency (Hz) experimental curve is obtained see Figure 4.3, keeping the same input voltage. The experimental tests, according to this method, are performed to evaluate the piezoelectric performance in application involving closed air circulation.

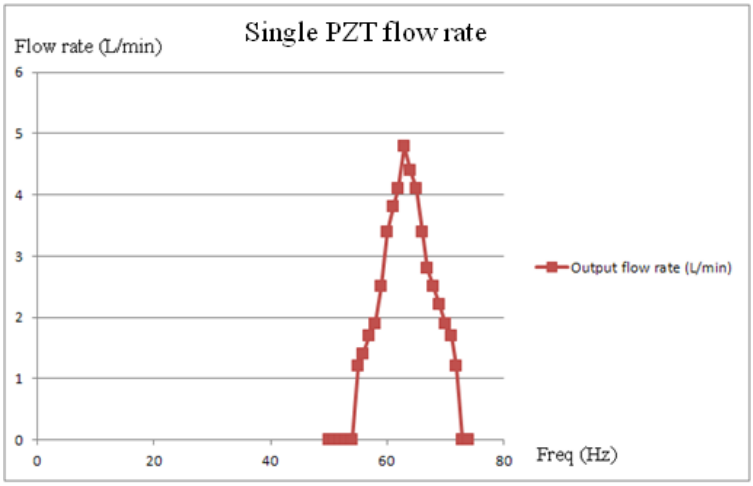

Figure 4. 3 Measured flow rate versus frequency curve

The result values obtained from experimental prototype has been verified as follows. To decrease the outlet size until reached 1.6 cm, the result is obviously higher than the normal size of outlet (2.6cm), as shown in Figure 4.4 red dots.

Oppositely, if keeping the outlet size is the same (2.6cm), and decreased the inlet size (2.6cm reduce to 0.4cm), the maximum output result obtained while the inlet size is 0.6 cm, as shown in Figure 4.5 blue dots.

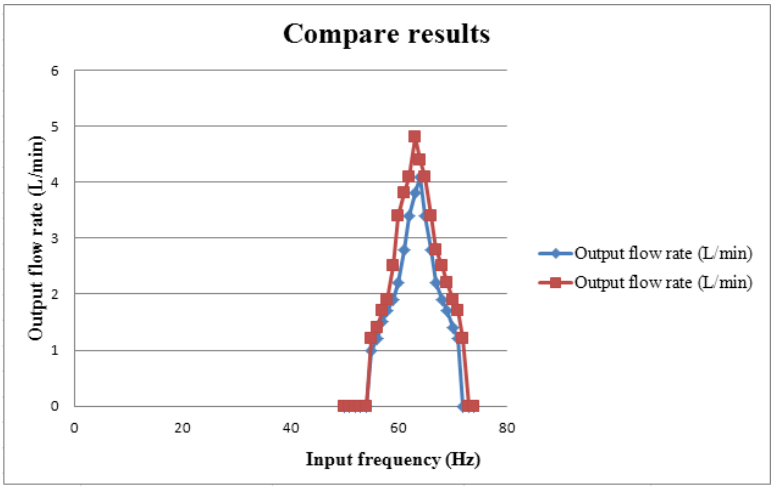

Figure 4. 4 Decreased the outlet gap

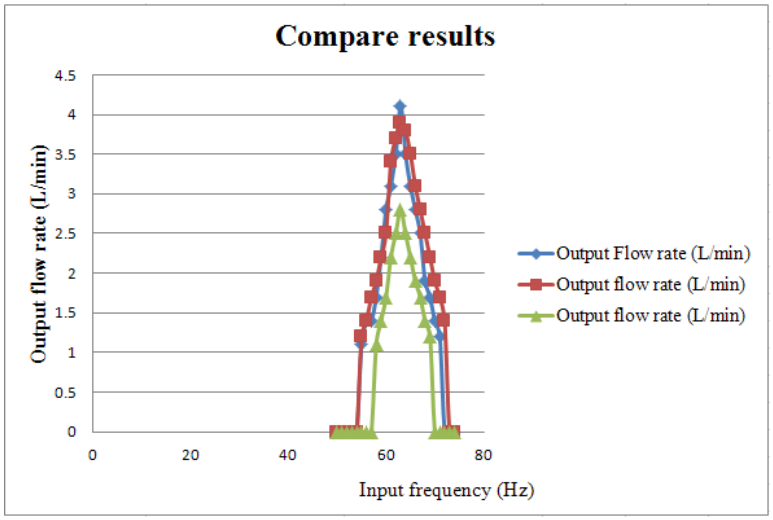

Figure 4. 5 decreased the inlet gap

As expected, the way of control inlet and outlet is important factor to obtain the maximum air flow. As shown in Figure 4.4 and 4.5, the maximum flow rate increase with input frequency, before its attained 60 Hz, after then, the output flow rate will decrease.

The preformed test (Figure 4.4) shows that the average of maximum flow rate

archived is 4.8L/min, at the resonance frequency of 60 Hz, with 115 V AC power input. It is clear to see that the maximum flow rate happened if the outlet gap was decreased. In order to make a compare between the special shape (trapezoidal) and normal shape (rectangle), the piezoelectric fan assemble is designed to maintain small gap between the vibrating fan and the outlet. Therefore, the outlet dimensions for each case are slightly larger than the fan width and two times the vibration amplitude in the horizontal and vertical dimensions **[61]**. See Figure 4.6.

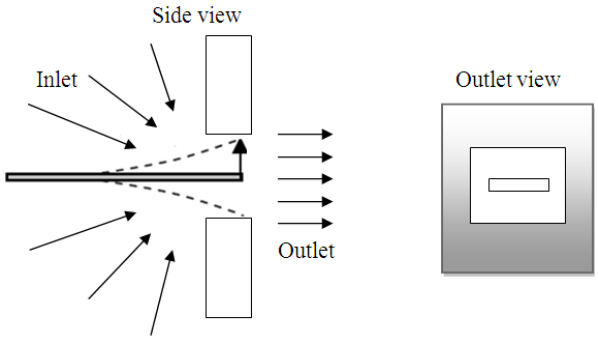

Figure 4. 6 Illustrations of piezoelectric fan assembly used during experimentation

The piezoelectric fan considered in the work has a width 1.27cm; therefore, the outlet width for the final design is set to 1.5cm, which leaves 2mm gap between the vibrating fan and casing in the horizontal direction. The height of the outlet is adjusted to be 2mm larger on each side than the vibration amplitude.

4.4 Two piezoelectric fans in parallel and series configuration testing results

The experimental prototypes which are built considering two piezoelectric fans in parallel and in series configuration, respectively. The pump prototype for parallel configuration is composed by two piezoelectric fans allocated inside a channel constructed in a pair of symmetrical parts, results as shown in Figure 4.7.

In the prototype for series configuration two piezoelectric fans are positioned in the same straight line, obtained results as shown in Figure 4.8.

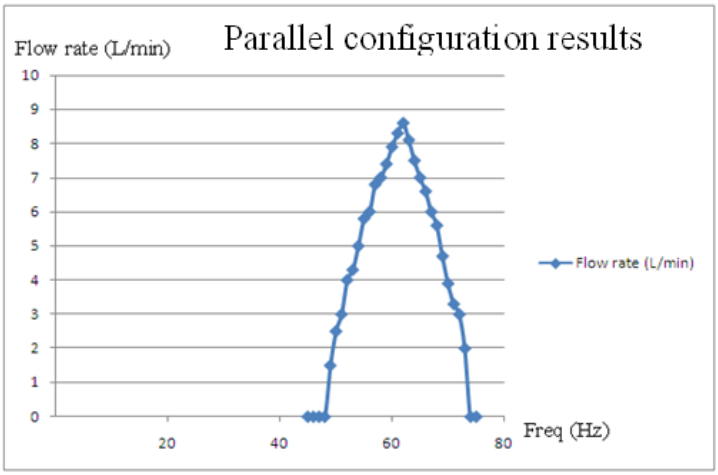

Figure 4. 7 The flow rate of parallel configuration

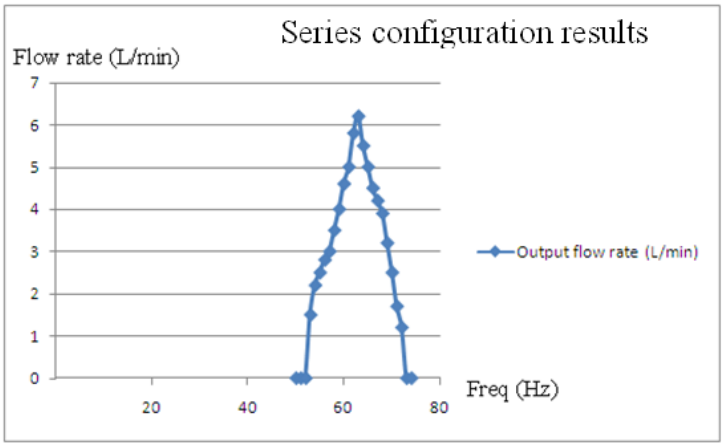

Figure 4. 8 The flow rate of series configuration

According to results obtained in this present work, for parallel configuration a maximum flow rate equal 8.6L/min, and it is much higher than the series configuration 6.3L/min.

4.5 The double piezoelectric fan testing resulting

The new micropump (double piezoelectric fan) indicates the range of input frequency from 50 to 75 Hz provides a corresponding increase in air flow rate from 0 L/min up

to 72 L/min (1.2 L/s) and air pressure from 0 Pa to 0.16 Pa. as shown in Figure 4.9 and Figure 4.10.

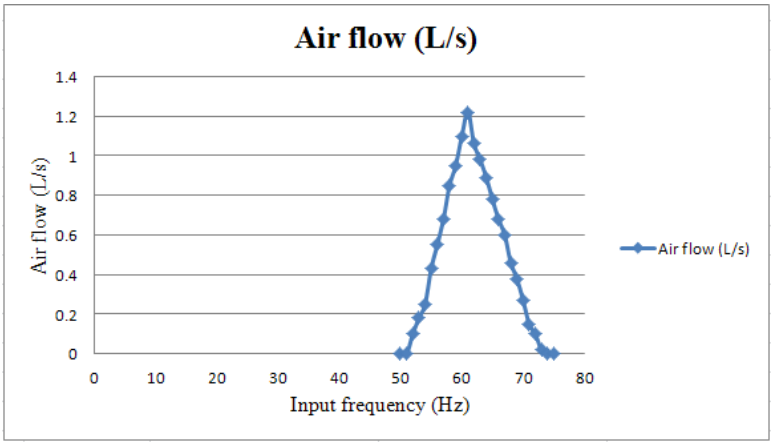

Figure 4. 9 Measured flow rate versus input frequency

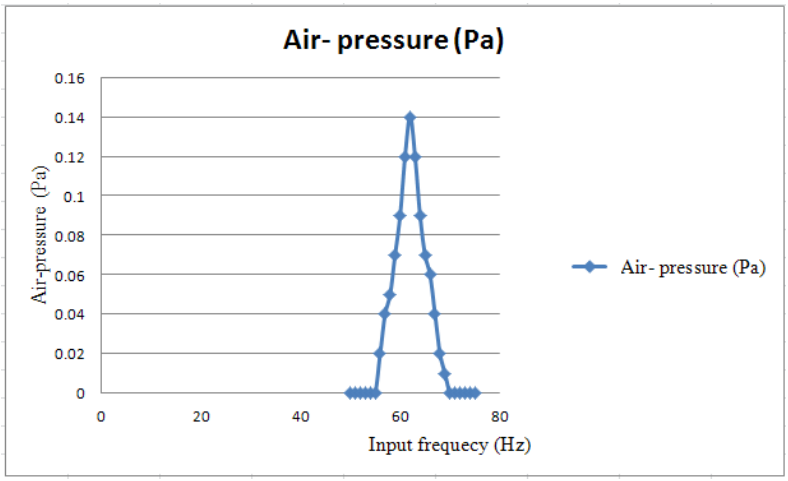

Figure 4. 10 Measured air pressure versus frequency

For comparing the new prototype results with previous experiment results, the maximum flow rate is higher than the single piezoelectric fan and two piezoelectric fan in parallel configuration, it is completed the first objective of this project to achieve the maximum flow rate 60 L/min ~ 90 L/min (1 L/s ~ 1.2 L/s). However, that air-pressure value is still not enough to provide higher pressure to deliver air and droplets into nasal mask.

4.6 Fluid flow and air-pressure analysis

According to air pressure results of these simulations considering two piezofans in parallel and series configuration for pump system are described along this section.

4.6.1 Results considering two parallel configuration piezofans

As below Figure 4.11 shows the model applied for fluid flow simulation of the pump system considering two parallel piezofans **[62]**. The resonance vibration mode, considering the fluid environment around the piezofan, has a frequency equal to 60 Hz with maximum amplitude of 2.54 cm at free ends of piezofans for a 115 Vpp (peak-to-peak applied voltage).

In Figure 4.11 shows the adopted FE mesh, which contains 15,958 nodes, and it illustrates details about pump channel model at inlet and outlet regions. Boundary conditions such as piezofan clamps (fixed nodes), channel walls, and specified displacements and fluid velocities are adopted for the model. In this case, nodes belonging to top and bottom line of the channel have null displacement and velocity, while nodes belonging to piezofans assume the displacement and velocity obtained from the piezoelectric actuator analysis. Null relative pressures are specified at inlet and outlet areas, since it is considered a total submerged pump and horizontal fluid flow.

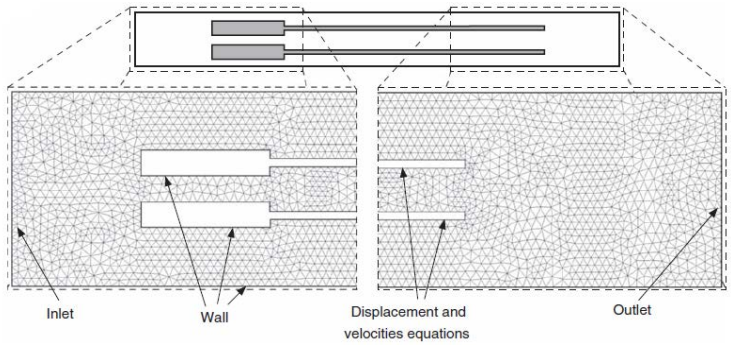

Figure 4. 11 The finite element mesh for fluid simulation [65]

To evaluate the average flow rate as frequency of excitation is changed, the optimized value shown in Figure 4.12 is adopted $\boldsymbol{H_{gap}}$ = 2.5cm. The plot of Figure 4.13 describes the results obtained from this evaluation for the distance between two walls on Mylar part, the range is 0~12cm, in which the maximum flow rate value is found at 8cm. In Figure 4.14 shows curve to depict the maximum flow rate obtained from experimental while the distance between two walls on piezoelectric material part (5.5cm). The pump performance changed when the cross sections of the inlet and outlet are enlarged. According to mass conservation, the velocity near the valve decreases due to the wider cross section. It is implicated not in the vibration of the valves but also in the damping force in the inlet and outlet.

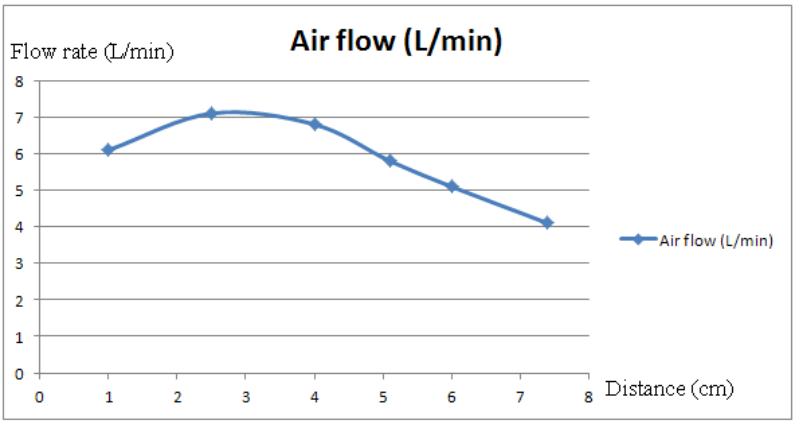

Figure 4. 12 Flow rate vs. the distance between two piezofans

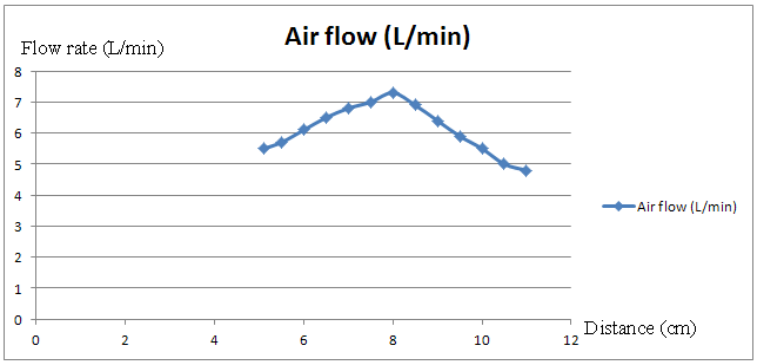

Figure 4. 13 Flow rate vs. the distance between two walls on Mylar part

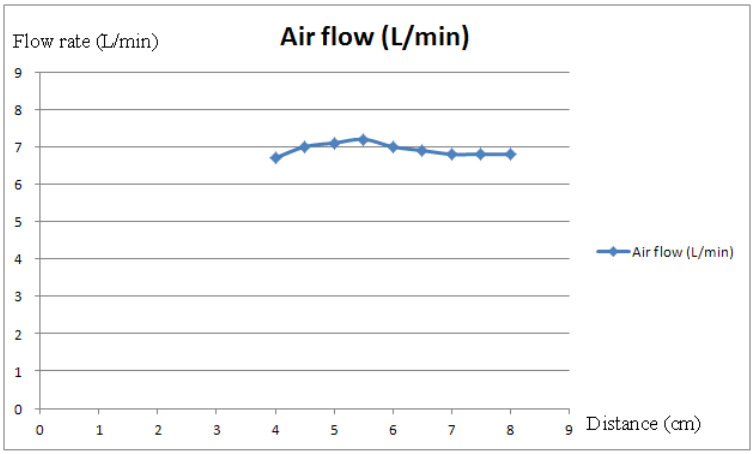

Figure 4. 14 Flow rate vs. the distance between two walls on PZT part

4.6.2 Results considering two series configuration piezofans

As the Figure 4.15 shows the model applied for fluid flow simulation of the pump system considering two series piezofans, it contains 16,000 nodes and boundary conditions are similar to the ones adopted for parallel configuration model described in the above section "*Results Considering Two Parallel Configuration Piezofans*".

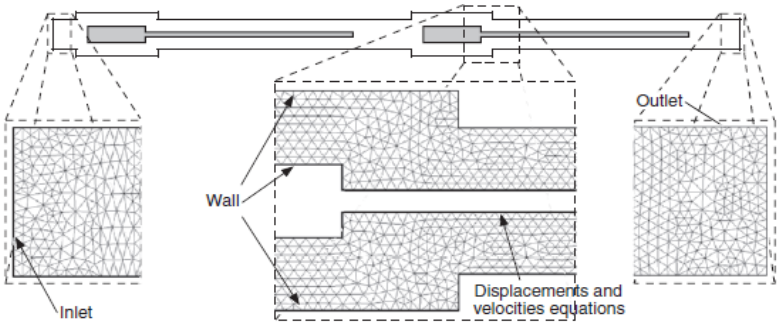

Figure 4. 15 The finite element mesh for fluid simulation in cascade configuration [66]

The curve shows in Figure 4.16, the same distance and input frequency defined for $\boldsymbol{L_{gap}}$ = 5cm can be used in following fluid flow simulation, which model is depicted in Figure 4.15. When $\boldsymbol{L_{gap}}$ than 5cm, the maximum flow rate (4.8 L/min) decrease, due to returned flow rate region between two series piezofans in cascade configuration. For value larger than 5 cm they also decrease due to load loss at channel walls, see Figure 4.16.

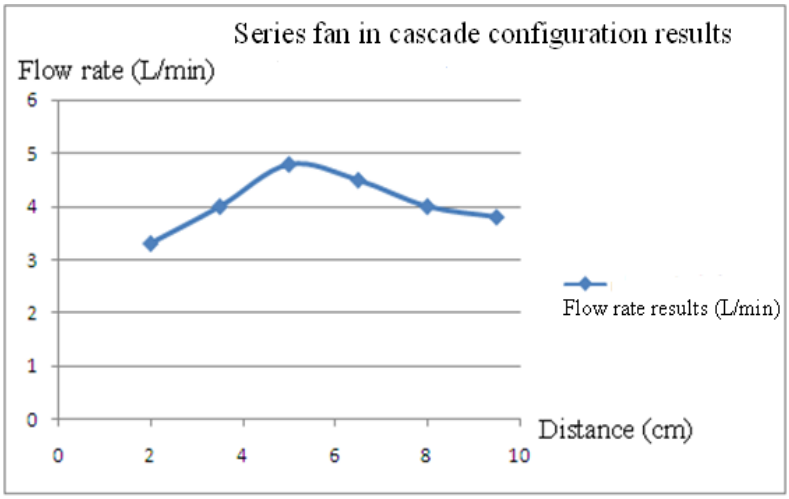

Figure 4. 16 The flow rate vs. distance between two series fans in cascade configuration

To evaluate the maximum flow rate as a function of excitation frequency, the optimized model (L_{gap} 5cm) is adopted. Figure 4.17 depicts the results obtained from this evaluation, in which the maximum flow rate of 6.1 L/min is found at resonance frequency (60 Hz).

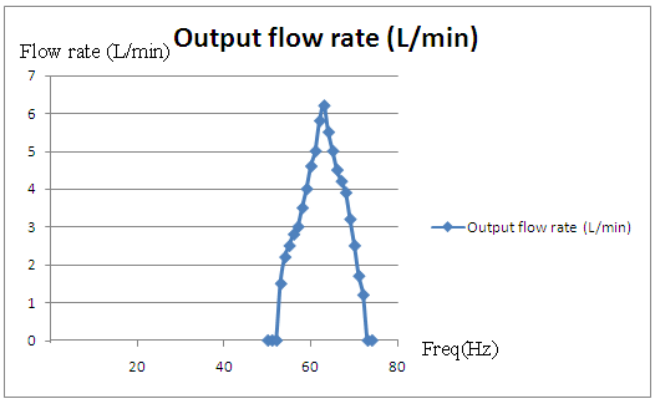

Figure 4. 17 The flow rate vs. varying frequency for series configuration in cascade

4.6.3 Compare results for parallel and series configurations

As Figure 4.18 shows the diagram of two parallel configuration Piezofans pressure head vs. two series configuration, and considering the distance between two fans is equal 2 cm (Parallel) and 2.5cm (series), which displays maximum pressure head of 0.3 Pa in series connected and 0.2 Pa in parallel connected at 60 Hz. Because when

the flow encounters obstacles of the components (series configuration), the pressure inside the pump chamber becomes higher, and it expands the volume inside the pump. This increased pressure pushes and consequently affects the piezoelectric device and the pump main body. It leads to an improper vibration of the piezoelectric device and results in a flow rate decrease.

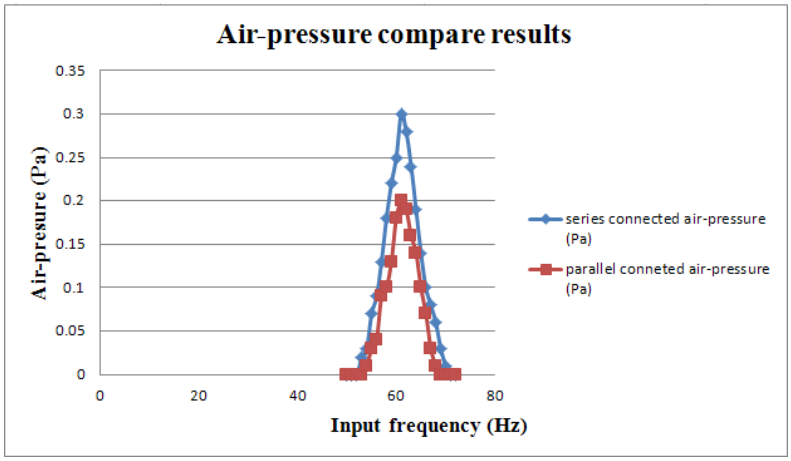

Figure 4. 18 Compare two air pressures between series and parallel configuration

Therefore, a pump with a higher flow rate does not guarantee a higher pump head, the performance depends on the correlation among the piezoelectric device, and the pump chamber.

As expected, the maximum pressure and flow rate both increase with amplitude. The general relationship between pressure and flow rate is readily observed by normalized each curve with its respected maximum values. This result is shown in Figure 4.19 and suggests that P (air pressure) -Q (air flow rate) diagram could be estimated with an equation of the form.

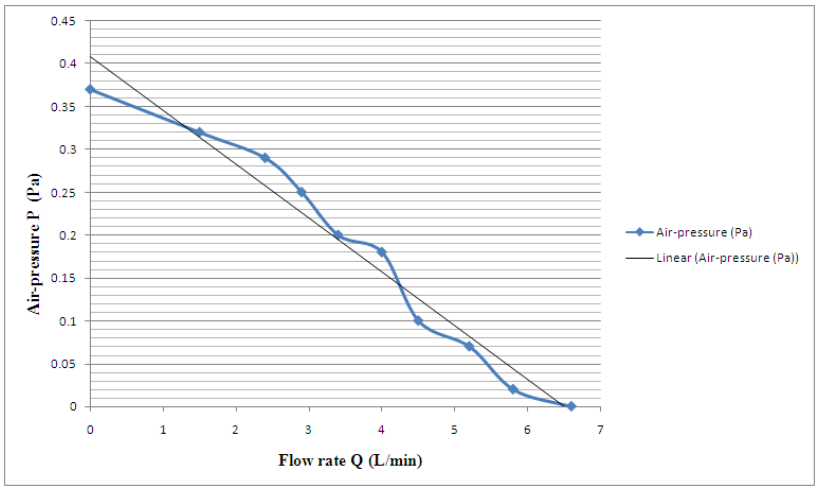

Figure 4. 19 The general relationship between pressure and flow rate

$$P = -0.0628Q + 0.4078 \quad (3.1)$$

4.7 Summary

According the previous work presented, there is a frequency range in which it is possible to obtain approximately a parabola change of air flow and air pressure by just varying the excitation frequency of the piezoelectric fans. By improving the shape of chamber and the position of piezoelectric fans, this parameter can be a way to control air flow and air pressure of the micropump.

Chapter 5 Discussion and Conclusions

5.1 Introduction

This chapter provides discussion for the system investigation in Chapter 3 and the experimental results presented in Chapter 4. The airflow generation of micropump for the CPAP system is discussed, with trends in the dominant mechanisms being identified.

5.2 Preliminary investigation

A preliminary experiment was performed in the presented work to determine whether it was possible to develop a new concept micropump that could be used as basis for comparison again the tradition micropump in the CPAP system. To find out a suitable devices to assemble the micropump, the experiment is used a single piezoelectric fan was placed inside an air-tight chamber, with input signal 115 V AC and 60 Hz, resulting in a maximum flow and air pressure are very low. When two piezofans connected together in parallel or series configuration, they will provide larger flow rates and larger air-pressures. As expected, the maximum pressure and flow rate both increase with amplitude and structure. However, the pressure is highest at the zero flow rate condition and then decreases monotonically until the maximum flow rate is reached at the zero pressure condition, obviously the general relationship between flow rate and pressure is oppositely, if this research project wants obtain higher flow rate, then air pressure will drop lower, which means the micropump couldn’t deliver air flow and droplets into mask. Therefore, personally believe the second piezoelectric fan (double piezoelectric fan) is the suitable device; it can be used in the future design.

5.3 Conclusions

The purpose of this thesis was to develop an Air Believer Unit in the CAPA system by selecting a suitable piezoelectric fan, characterizing it through experimentation, designing adapt its micropump, analyzing the air flow and air pressure, then defining global characteristics of the whole system. This thesis has met these objectives. The findings of this thesis suggest that:

a. The vibration frequency is more influential in determining the air flow and air pressure compared to the vibration amplitude.

b. The parallel configuration of two piezofans excited with same phase yields more flow rate than excited with opposite phase. And the parallel configuration yields more flow rate than series configuration, but the series configuration yields higher air pressure.

c. The shapes of channel, inlet and outlet have relatively influence on the flow rate or air pressure.

d. The material of piezoelectric fan (mylar or steel or other material) is determining the resonance frequency and the maximum amplitude of piezoelectric fan.

5.4 Future design

In order to complete the development of this micropump, work needs to be done include an enhancement of the maximum air pressure, improving piezoelectric fan for running under NZ power supply, and other configurations using difference piezoelectric fans.

APPENDIXES A

Because the damping ration is related to the logarithmic decrement δ for underdamped vibrations via the relation

$$\zeta = \frac{\delta}{\sqrt{(2\pi)^2 + \delta^2}} \qquad \text{where} \qquad \delta \triangleq \ln \frac{x_1}{x_2}.$$

This relation is only meaningful for underdamped systems because the logarithmic decrement is defined as the natural log of the ratio of any two successive amplitudes, and only underdamped systems exhibit oscillation

Firstly, the experimental is needs to set up by the oscilloscope and vibrameter, select the range of vibrameter (5260 μm/V), then make the laser point to the Mylar (PZT). Secondly, touch the Mylar quickly and gently, record the first and second amplitude average values (15 times):

1. $\delta = \ln \frac{X_1}{X_2}$ $\delta = \ln \frac{202}{194}$ $\delta = 0.04$
2. $\delta = \ln \frac{X_1}{X_2}$ $\delta = \ln \frac{168}{158}$ $\delta = 0.061$
3. $\delta = \ln \frac{X_1}{X_2}$ $\delta = \ln \frac{136}{128}$ $\delta = 0.061$
4. $\delta = \ln \frac{X_1}{X_2}$ $\delta = \ln \frac{184}{176}$ $\delta = 0.044$
5. $\delta = \ln \frac{X_1}{X_2}$ $\delta = \ln \frac{170}{160}$ $\delta = 0.061$
6. $\delta = \ln \frac{X_1}{X_2}$ $\delta = \ln \frac{152}{146}$ $\delta = 0.040$
7. $\delta = \ln \frac{X_1}{X_2}$ $\delta = \ln \frac{164}{156}$ $\delta = 0.05$

8. $\delta = \ln\frac{X_1}{X_2}$ $\delta = \ln\frac{164}{158}$ $\delta = 0.036$ **(error)**

9. $\delta = \ln\frac{X_1}{X_2}$ $\delta = \ln\frac{178}{170}$ $\delta = 0.046$

10. $\delta = \ln\frac{X_1}{X_2}$ $\delta = \ln\frac{170}{162}$ $\delta = 0.048$

11. $\delta = \ln\frac{X_1}{X_2}$ $\delta = \ln\frac{204}{194}$ $\delta = 0.05$

12. $\delta = \ln\frac{X_1}{X_2}$ $\delta = \ln\frac{160}{152}$ $\delta = 0.051$

13. $\delta = \ln\frac{X_1}{X_2}$ $\delta = \ln\frac{188}{178}$ $\delta = 0.055$

14. $\delta = \ln\frac{X_1}{X_2}$ $\delta = \ln\frac{164}{154}$ $\delta = 0.063$ **(error)**

15. $\delta = \ln\frac{X_1}{X_2}$ $\delta = \ln\frac{158}{150}$ $\delta = 0.052$

The average of the δ for the Mylar is equal to 0.0506

Considering the second part of the whole system, which is only include the Mylar, used a tool to hold the PZT part, let the second part is become to a one – degree vibration cantilever beam as shown at the below diagram.

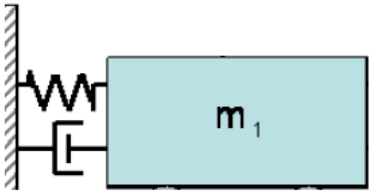

(1). $\zeta = \frac{\delta}{\sqrt{(2\Pi)^2+\delta^2}} = \frac{0.0506}{\sqrt{(2\Pi)^2+0.0506^2}} = 0.00805$ *(Damping ratio of the Mylar)*

(2). $\omega_d = \frac{2\pi}{T} = \frac{2\pi}{0.017} = 369.58$ rad/s *(Damping natural frequency)*

(3). $\omega_d = \omega_n\sqrt{1-\xi^2}$

$\omega_n = \frac{\omega_d}{\sqrt{1-\xi^2}}$

$\omega_n = \frac{369.58}{\sqrt{1-0.00805^2}}$

$\omega_n =$ 369.59 rad/s

(4). $f_n = \frac{\omega_n}{2\pi} = \frac{369.59}{2\pi}$ = 58.82 Hz *(The resonance frequency)*

(5). m = ρ V

= 1.3925 g/cm^3 (the density of Mylar) x 3.6cm x 1.27 x 0.053 cm

= 0.337g

= 0.000337kg

(6). W $_{(Mylar)} = \frac{m}{L} = \frac{0.000337Kg}{0.036m}$ = 0.00937 Kg/m *(The weight of length of Mylar)*

(7). M = $\frac{30}{140}$ WL

= $\frac{30}{140}$ x 0.00937 Kg/m x 0.036 m

= 0.0000723 Kg *(The equivalent mass of Mylar)*

(8). When the resonance frequency is equal f_n = 58.82 Hz.

$\omega_n = 2\pi f_n$

= 2 π x 58.82Hz

=369.59 rad/s

(9). $\omega_n = \sqrt{\frac{K}{m}}$

$K_{mylar} = \omega_n^2$ m

= 3.69.59 rad/s x 0.0000723

= 9.88 N/m (*The spring constant of Mylar)*

(10). $\xi = \frac{C}{2\sqrt{Km}}$

$C = 2\xi\sqrt{Km}$

C = 2 x 0.00805 x $\sqrt{9.88 \times 0.0000723}$

C= 0.00043 Kg/s *(The damping coefficient of Mylar)*

APPENDIXES B

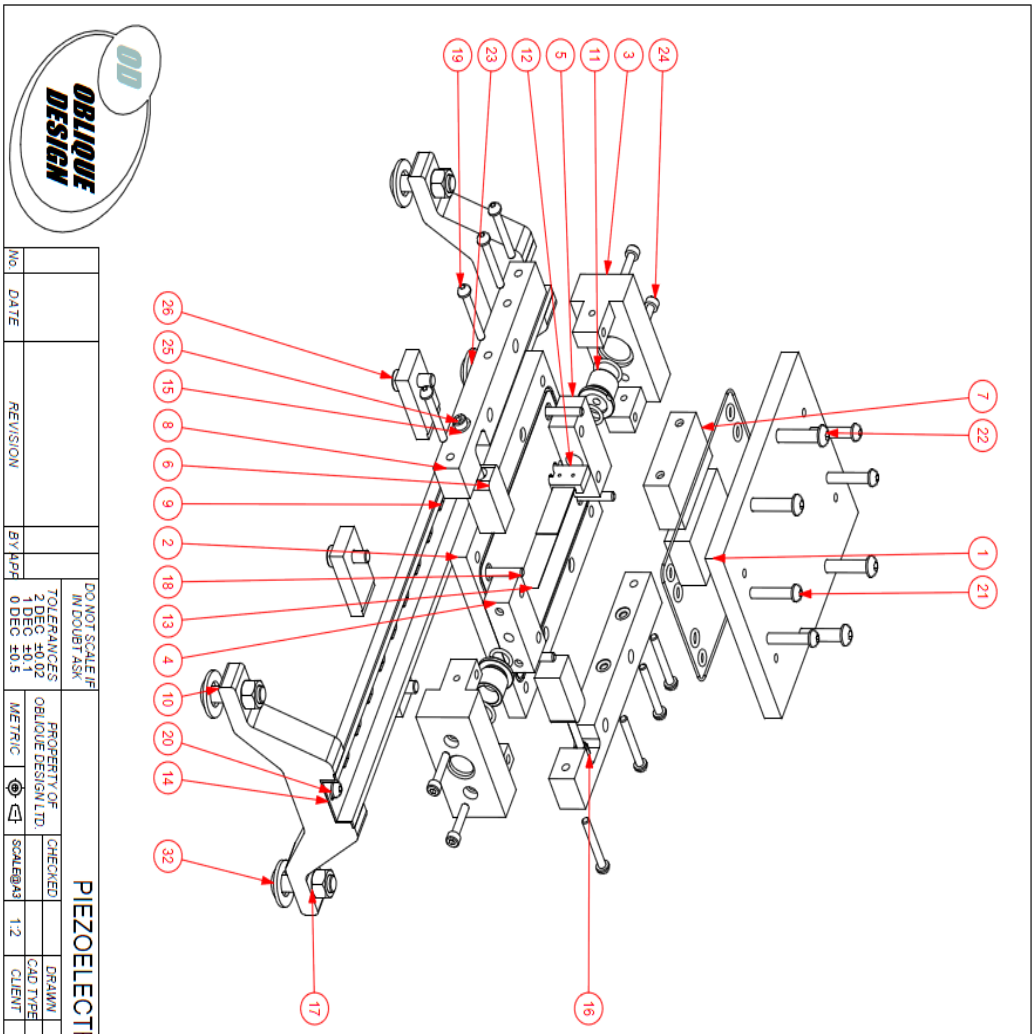

ITEM NO.	PART NO.	DESCRIPTION	QTY IN MODEL
1	101	TOP CAP PLATE	1
2	102	BOTTOM CAP PLATE	1
3	103	ENDCAP	2
4	104	OUTLET DIFFUSER	1
5	105	INLET DIFFUSER	1
6	106	TIP INTERACTION BLOCK	2
7	107	INLET BLOCK	2
8	108	OUTER WALL	2
9	109	CLAMP	4
10	110	FOOT	2
11	111	LINE FITTING	2
12	113	BLADE MOUNT	1
13	115 VAC / 60 HZ	PIEZOELECTRIC FAN	1
14	36 MM	DIN RAIL	1
15	4 MM	WASHER	2
16	4 MM	NYLOCK NUT	2
17	8 MM	METRIC NUT	4
18	4 X 25	DOWEL	4
19	4 x 30	DOMEHEAD CAP SCREW	8
20	5 x 20	DOMEHEAD CAP SCREW	2
21	5 x 35	DOMEHEAD CAP SCREW	4
22	6 x 35	DOMEHEAD CAP SCREW	4
23	8 x 30	DOMEHEAD CAP SCREW	4
24	4 x 20	SOCKET HEAD CAP SCREW	4
25	4 x 35	SOCKET HEAD CAP SCREW	2
26	6 x 16	SOCKET HEAD CAP SCREW	4
27	007	O RING	2
28	008	O RING	8
29	009	O RING	4
30	012	O RING	2
31	014	O RING	2
32	112	RUBBER PAD	4
33	048	O RING	2

OBLIQUE DESIGN

No.	DATE	REVISION	BY	APP

DO NOT SCALE IF IN DOUBT ASK

TOLERANCES
2 DEC ±0.02
1 DEC ±0.1
0 DEC ±0.5

PROPERTY OF OBLIQUE DESIGN LTD.

METRIC

CHECKED

SCALE@A3: 1:2

DRAWN: PMW

CAD TYPE: SOLIDWORKS

CLIENT: AUT

DATE: 11/10/2010

JOB NO.: 1001

DRW NO.: 100

REV: 0

SHT 2 / 2

PIEZOELECTRIC PUMP DEVICE

QTY: 1

FINISH

PART MAT.

TREATMENT

Reference

1. Young, T., et al., *The occurrence of sleep-disordered breathing among middleaged adults.* New England Journal of Medicine, 1993. **328**(17): p. 1230-1235. (Accessed date: 20.11. 2010)
2. Lam, B., D.C.L. Lam, and M.S.M. Ip, *Obstructive sleep apnoea in Asia.* International Journal of Tuberculosis and Lung Disease, 2007. **11**(1): p. 2-11. (Accessed date: 20.11. 2010)
3. Ip, M.S.M., et al., *A Community Study of Sleep-Disordered Breathing in Middle-Aged Chinese Women in Hong Kong: Prevalence and Gender Differences.* Chest, 2004. **125**(1): p. 127-134. (Accessed date: 20.11. 2010)
4. Udwadia, Z.F., et al., *Prevalence of Sleep-disordered Breathing and Sleep Apnea in Middle-aged Urban Indian Men.* American Journal of Respiratory and Critical Care Medicine, 2004. **169**(2): p. 168-173. (Accessed date: 20.11. 2010)
5. Young, T., et al., *The occurrence of sleep-disordered breathing among middleaged adults.* New England Journal of Medicine, 1993. **328**(17): p. 1230-1235. (Accessed date: 20.11. 2010)
6. Ralph Downey III, *Obstructive Sleep Apnea Treatment & Management* (Accessed date: 22.11. 2010)
7. Ralph Downey III, *Obstructive Sleep Apnea Treatment & Management* (Accessed date: 22.11. 2010)
8. Ralph Downey III, *Obstructive Sleep Apnea Treatment & Management* (Accessed date: 22.11. 2010)
9. *Sleep Apnea and Snoring* (Accessed date: 22.11. 2010)
10. *Sleep Apnea and Snoring* (Accessed date: 22.11. 2010)
11. *Sleep Apnea and Snoring* (Accessed date: 22.11. 2010)
12. *Positive airway pressure* (Accessed date: 22.11. 2010)
13. Mintz, M.L., *Disorders of the Respiratory Tract: Common Challenges in Primary Care*. 2006: Humana Press. (Accessed date: 22.11. 2010)
14. Ian R. Henderson: *Piezoelectric Ceramics Principle and Applications*, (pp. 6-7, 2003)

15. Mark Kimber, Kazuhiko Suzuki, Nobutaka Kitsunai, Kenichi Seki, Suresh Garimella: *Pressure and Flow Rate Performance of Piezoelectric Fans*, (pp.1-2, 2009) (Accessed date: 09.12. 2010)
16. Tolga Acikalin, Suresh.V. Garimella and Arvind Raman: *Experimental Investigation of the Thermal Performance of Piezoelectric fans*, *Heart Transfer Engineering Copyright Taylor& Francis Inc* 25(1): 4-14, 2004. (Accessed date: 11.12. 2010)
17. Toda, M., Voltage-*induced Large amplitude bending device PVF_2 Bimorph – Its properties and applications*, Ferroelectrics, (vol, 32 pp. 127-133, 1981.) (Accessed date: 11.12. 2010)
18. Yoo, J. H., J. I., and Cao, W., *Piezoelectric Ceramic Bimorph Coupled to thin Metal Plate as Cooling Fan for Electronic Device*, *Sensors and Actuators A*, (vol. 79,pp. 8 – 12, 2000.) (Accessed date: 11.12. 2010)
19. Schmid, R. R., *Local and Average Transfer Coefficients on Vertical Surface Due to Convection from A piezoelectric Fan*, Inter Society Conference on Thermal Phenomena, (pp. 41 – 49, 2000.) (Accessed date: 11.12. 2010)
20. Ihara, A., and Watanabe, H., *On the Flow around Flexible Plates, Oscillating with Large Amplitude*, Journal of Fluids and Structures, (vol. 8 pp. 601 – 619, 1994.) (Accessed date: 11.12. 2010)
21. Piezo System, INC. Catalogue 7 datasheet, (pp, 12) (Accessed date: 18. 12. 2010)
22. Ian R. Henderson: *Piezoelectric Ceramics Principle and Applications*, (pp. 13 - 20, 2003) (Accessed date: 18. 12. 2010)
23. 1. Bernard Jaffe: Piezoelectric ceramics (pp.9-16. 1985)
    2. Sydney M. Wait, Sundipta Basak, Suresh V.Garimella, and Arvind Raman: Piezoelectric Fans Using Higher Flexural Modes for Electronics Cooling Application (pp. 119-124)
24. Ing. Petr SEDLÁK and Štěpán HEFNER: *PIEZOELECTRIC SENSORS: BASIC MODELS*, (pp, 2 – 5, 2002)
25. Daniel J. Inman: *Engineering Vibration* second edition, (pp, 243 - 267)
26. Daniel J. Inman: *Engineering Vibration* second edition, (pp, 384 - 388)
27. Piezo System, INC. Catalogue 7 datasheet, (pp, 57-59)
    Accessed date 20.12.2010)

28. Ian R. Henderson: *Piezoelectric Ceramics Principle and Applications*, (pp. 44 - 48).

29. Daniel J. Inman: *Engineering Vibration* second edition, (pp, 243 - 267)

30. 1. Cicero R. de Lima, Sandro L. Vatanabe, Andres Choi, Paulo Henrique Nakasone: Sensors and Actuators A: Physical – A biomimetic piezoelectric pump: computational and experiemental chararcterization (pp. 2-4)

    2. Sandro L. Vatanabe, Andres Choi, Cicero R. de Lima and Emilio Carlos Nelli Silva: Jounrnal of Intelligent Material Systems and Structures (pp. 2-5)

    3. Cicero R. de Lima, Sandro L. Vatanabe, Andres Choi, Paulo Henrique Nakasone: Sensors and Actuators A: Physical – A biomimetic piezoelectric pump: computational and experiemental chararcterization (pp. 1-3)

31. Mark Kimber, Kazuhiko Suzuki, Nobutake Kitsunal, Kenichi Seki, Suresh Garimella: Pressure and Flow Rate Performance of Piezoelectric Fans (Vol 32 No.4 Dec, Year2009)

32. Sandro L. Vatanabe, Andres Choi, Cicero R. de Lima and Emilio Carlos Nelli Silva: *Design and Characterization of a Biomimetic Piezoelectric Pump Inspired on Group Fish Swimming Effect*, Jounrnal of Intelligent Material Systems and Structures (Vol.21, pp.133 – 135 Jan. 2010)

33. Sandro L. Vatanabe, Andres Choi, Cicero R. de Lima and Emilio Carlos Nelli Silva: *Design and Characterization of a Biomimetic Piezoelectric Pump Inspired on Group Fish Swimming Effect*, Jounrnal of Intelligent Material Systems and Structures (Vol.21, pp.134 – 136 Jan. 2010)

34. Sandro L. Vatanabe, Andres Choi, Cicero R. de Lima and Emilio Carlos Nelli Silva: *Design and Characterization of a Biomimetic Piezoelectric Pump Inspired on Group Fish Swimming Effect*, Jounrnal of Intelligent Material Systems and Structures (Vol.21, pp.136 - 138 Jan. 2010)

35. Piezoelectric Ceramics: Principles and Applications (pp. 44 - 46)

36. Mark Kimber, Kazuhiko Suzuki, Nobutake Kitsunal, Kenichi Seki, Suresh Garimella: Pressure and Flow Rate Performance of Piezoelectric Fans (Vol 32 No.4 Dec, Year2009)

37. Sandro L. Vatanabe, Andres Choi, Cicero R. de Lima and Emilio Carlos Nelli Silva: *Design and Characterization of a Biomimetic Piezoelectric Pump Inspired on Group Fish Swimming Effect*, Jounrnal of Intelligent Material Systems and Structures (Vol.21, pp.136 - 138 Jan. 2010)

38. Sandro L. Vatanabe, Andres Choi, Cicero R. de Lima and Emilio Carlos Nelli Silva: *Design and Characterization of a Biomimetic Piezoelectric Pump Inspired on Group Fish Swimming Effect*, Jounrnal of Intelligent Material Systems and Structures (Vol.21, pp.142 - 143Jan. 2010)
39. Sandro L. Vatanabe, Andres Choi, Cicero R. de Lima and Emilio Carlos Nelli Silva: *Design and Characterization of a Biomimetic Piezoelectric Pump Inspired on Group Fish Swimming Effect*, Jounrnal of Intelligent Material Systems and Structures (Vol.21, pp.145 -146 Jan. 2010)
40. Sandro L. Vatanabe, Andres Choi, Cicero R. de Lima and Emilio Carlos Nelli Silva: *Design and Characterization of a Biomimetic Piezoelectric Pump Inspired on Group Fish Swimming Effect*, Jounrnal of Intelligent Material Systems and Structures (Vol.21, pp.145 -146 Jan. 2010)